Hybrid LEGO-EFIE method applied to antenna problems comprising anisotropic media

Hybrid LEGO-EFIE Method Applied to Antenna Problems Comprised of Anisotropic Media

V. Lancellotti[(1)], D. Melazzi[(2)]
[(1)]Faculty of Electrical Engineering, Eindhoven University of Technology,
Eindhoven, The Netherlands
(e-mail: v.lancellotti@tue.nl)
[(2)]Department of Industrial Engineering, University of Padova,
Padova, Italy
(e-mail: davide.melazzi@gmail.com)

***Abstract*—Linear embedding via Green's operators (LEGO) is a domain decomposition method in which complex radiation and scattering problems are modelled and solved by means of interacting electromagnetic "bricks". We propose an extension of LEGO able to handle bodies with anisotropic constitutive parameters and metallic objects (e.g., antennas). Since the anisotropic objects are dealt with LEGO, and the metallic parts are treated with the electric field integral equation (EFIE), we refer to the overall approach as hybrid LEGO-EFIE. The characterization of an electromagnetic brick which embeds an anisotropic object requires solving a volume integral equation (VIE). Since this procedure is carried out for each brick independently, the LEGO approach *per se* is extremely advantageous over the direct solution of a global VIE for all the bodies at once. Nonetheless, we further mix the hybrid LEGO-EFIE approach with the eigencurrents expansion method in order to tackle relatively larger problems. The technique is used to analyze a reconfigurable plasma antenna array (PAA) comprised of magnetized-plasma tubes placed around a two-dipole antenna array.**

***Index Terms*—Antennas, anisotropic media, surface integral equations, volume integral equations, equivalence principles, Method of Moments, domain decomposition, macro basis functions, eigencurrents, magnetized plasma, scattering operators, plasma antennas.**

I. Introduction

Media with anisotropic constitutive parameters exist in nature and have found applications such as in the fabrication of optical components [1]. Besides, nowadays artificial materials can be engineered, for instance, by inserting metallic or dielectric inclusions within a host dielectric matrix; then, if the distribution and orientation of the underlying inclusions is asymmetric, the resulting material is likely to exhibit anisotropic behaviour [2], [3]. Also, magnetized plasma discharges, which have been employed as metamaterials [4] and antennas [5], [6], under certain conditions can be described macroscopically in the spatial domain by means of a non-Hermitian dyadic permittivity [7].

Electromagnetic (EM) radiation and scattering problems, which simultaneously involve perfectly electrically conducting (PEC) objects and penetrable bodies with anisotropic properties, are better formulated in terms of coupled volume-surface integral equations (VSIE) (e.g., [7]–[11]) because Sommerfeld's radiations conditions [12], [13] are automatically accounted for by the integral operators. However, it is well known that, when solved numerically with the Method of Moments (MoM) [14], surface integral equations (SIE) [8], [15]–[18] and volume integral equations (VIE) [11], [19]–[24] invariably yield dense and possibly large matrices.

One way of coping with this issue consists of reducing the number of degrees of freedom and, thus, the size of the algebraic system to be inverted. Said reduction can be realized by either breaking the original EM problem into electrically "smaller" sub-problems or by adopting specialized basis functions devised *ad hoc* for the geometry at hand; combinations of both strategies are also possible. An incomplete list of the methods that implement these ideas are: the synthetic functions expansion (SFX) [25]–[29], the characteristic basis function method (CBFM) [30]–[39], and its multilevel version [40], [41], the equivalence principle algorithm [42]–[45] and the tangential equivalence principle algorithm (T-EPA) [46], [47], the generalised surface integral equation (GSIE) method [48], the eigencurrents expansion [49], [50], and the linear embedding via Green's operators (LEGO) method [51]–[56].

In this paper we propose an extension of the LEGO approach to the analysis of EM radiation and scattering problems comprised of PEC objects (e.g., antennas) and an aggregate of anisotropic bodies, as is sketched in Fig. 1a. Since the anisotropic objects are dealt with LEGO, while the metallic parts are treated with the standard electric field integral equation (EFIE) so as to gain more generality (the magnetic field integral equation alone would, in fact, limit the application to *closed* surfaces) we call the overall approach hybrid LEGO-EFIE [57].

The basic idea of the LEGO method [54], [56] is the modelling of a complex and possibly large structure by means of simple-shaped EM "bricks". In this way, the local geometrical complexities [55] and even elementary sources confined to the inside of the bricks [58] can be treated efficiently, though separately, from the interactions which take place among the various "distant" parts of a structure. The EM behavior of each brick is expressed in terms of surface scattering operators of equivalent current densities, whereas the multiple scattering that occurs among any two bricks is captured by means of

surface transfer operators. By combining these two ingredients we can rigorously formulate the original EM problem. For this reason, LEGO constitutes a type of domain decomposition technique applied to SIEs.

In principle, there is no limitation to the contents of an EM brick, but to handle the aggregate of anisotropic bodies of interest here, it is convenient to enclose each body (tagged medium ③) into a separate domain, as suggested in Fig. 1b. By the same token, the host material (labelled ② in Fig. 1b) that pads the inside of the bricks can be arbitrary [55]. This feature was exploited, for instance, to analyze dielectric waveguides in which confinement is provided by electromagnetic band-gaps [58], [59]. For the sake of simplicity, though, we restrict our discussion to the special case where medium ② and the homogeneous background (labelled ①) possess the same EM properties.

Furthermore, although the EM bricks can have any shape, defining bricks with different shapes for a given problem may be unwise for computational purposes, or even impractical sometimes. Actually, if the bricks have all the same shape — but not necessarily the same content — then, the numerical calculations of the scattering and transfer operators are facilitated because some intermediate results can be recycled, and this helps reduce the computational workload. Secondly, while for general distributions of objects in space [60] the shape of the bricks is not restricted at all, adopting identical and simple shapes may be necessary when one needs to stack the bricks tightly in a regular pattern so as to model, e.g., dielectric slabs with inclusions [59].

The formulation of the antenna problem of Fig. 1 with hybrid LEGO-EFIE was outlined in [61] for the special instance of isotropic bodies, whereas the standard LEGO method (i.e., in the absence of PEC antennas) applied to clusters of anisotropic objects was described in [62]. In this regard, it will be clear further on that the LEGO functional equations take on the very same form, irrespective of the nature of the EM problem *inside* the bricks. As a result, the hybrid LEGO-EFIE to be discussed here will be based on the same modified EFIE we deduced in [61]. By contrast, the calculation of the scattering operators — which implies the solution of the scattering problem inside the bricks — must perforce be updated in order to allow for the dyadic constitutive parameters of medium ③. In particular, this could be done by combining the integral representation of the EM fields over a brick's boundary with the equivalent variational formulation of Maxwell's differential equations within the brick (e.g., [63], [64]). Alternatively, we prefer to adopt an approach based on the MoM solution of a VIE for the anisotropic object [62], as this strategy is in keeping with the embedding philosophy, which has already been developed for PEC and isotropic bodies [54]–[56].

It should be noted that, since the anisotropic nature of the body inside a brick is rigorously accounted for by the relevant scattering operator, which is a *surface* operator, the very application of the LEGO algorithm provides a means for reducing the number of unknowns in the context of the MoM solution. More precisely, we need to solve at most as many independent and relatively "small" VIEs as the number of bodies; evidently, this task is far less computationally intensive and memory demanding than the inversion of a global VIE for the aggregate of objects as a whole. Nevertheless, for EM problems modelled with a moderate to large number of bricks, the algebraic counterpart of the LEGO functional equations can still be too large for inversion with direct solvers, such as the LU factorization [65]. Therefore, in an attempt to overcome the memory limitations that large matrices would pose, we combine the hybrid LEGO-EFIE approach with the eigencurrents expansion method (EEM) [54], [57], [61], [66].

Simply put, in the EEM the eigenfunctions of a brick's scattering operator are employed as a set of locally entire-domain basis functions to expand the unknowns (i.e., equivalent surface current densities) introduced over the boundary of a brick. Since ordinarily only few lower-order eigenfunctions [57] are sufficient to accurately represent the unknowns, the EEM allows compressing the algebraic system of LEGO and hence, speeding up the matrix filling phase and the inversion.

The rest of the paper is organized as follows. In Section II, we review the basic concepts of LEGO (II-A), introduce the relevant unknown current densities through the EM equivalence principles (II-B), derive the LEGO equations for the bricks (II-C), formulate the EFIE for the conducting parts of the problem (II-D), and deduce the modified EFIE (II-E). In Section III the derivation of scattering and transfer operators is discussed with a focus on bodies with anisotropic constitutive parameters. The numerical solution with the MoM and sub-sectional basis functions is outlined in Section IV, whereas the compression of the algebraic counterpart of the LEGO equations with EEM is the subject of Section V. The validation of the numerical implementation and the convergence of the EEM are presented in Section VI. As an example of application of hybrid LEGO-EFIE to a complex EM problem, in Section VII we investigate the radiation properties of a reconfigurable plasma antenna comprised of a two-dipole linear antenna array surrounded by cylindrical magnetized-plasma tubes.

Finally, a time-dependence in the form $\exp(\mathrm{j}\omega t)$ for fields and sources is assumed and suppressed throughout.

II. Formulation

A. Description of the problem and LEGO model

We are concerned with the solution of an EM radiation problem (Fig. 1a) which consists of a metallic multi-port antenna and $N_D \geq 1$ identical penetrable bodies immersed in a homogeneous unbounded background (medium ①). Our goal is to determine the network parameters (e.g., the impedance matrix) and the radiation pattern of the antenna-objects system.

The objects — which can have *arbitrary* shape and position in space — are made of an anisotropic material (medium ③) endowed with dyadic permittivity ($\overline{\overline{\varepsilon}}_3$) and permeability ($\overline{\overline{\mu}}_3$); let $\mathcal{V}_\mathrm{O}$ denote the region of space occupied by an object. As is customary, we assume the antenna and the other metallic parts, if any are present, to be perfect electrical conductors (PEC). We indicate with $\mathcal{V}_\mathrm{A}$ the volume occupied by the conductors and with $\mathcal{S}_\mathrm{A} \equiv \partial\mathcal{V}_\mathrm{A}$ the boundary thereof. Besides, for the

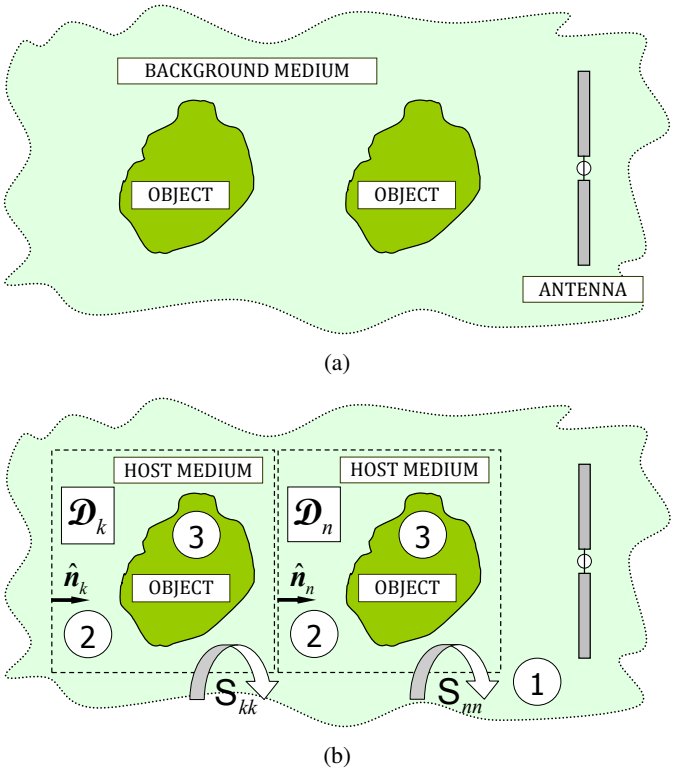

Fig. 1: EM problem and LEGO bricks: (a) a metallic antenna operating in the presence of N_D anisotropic bodies (medium ③); (b) in accordance with the LEGO approach, each object is embedded inside an EM brick $\mathcal{D}_k$, $k = 1, \ldots, N_D$, in turn described by means of a scattering operator S_{kk}. In this work we examine the special instance of background material (①) and host medium (②) endowed with the same constitutive parameters.

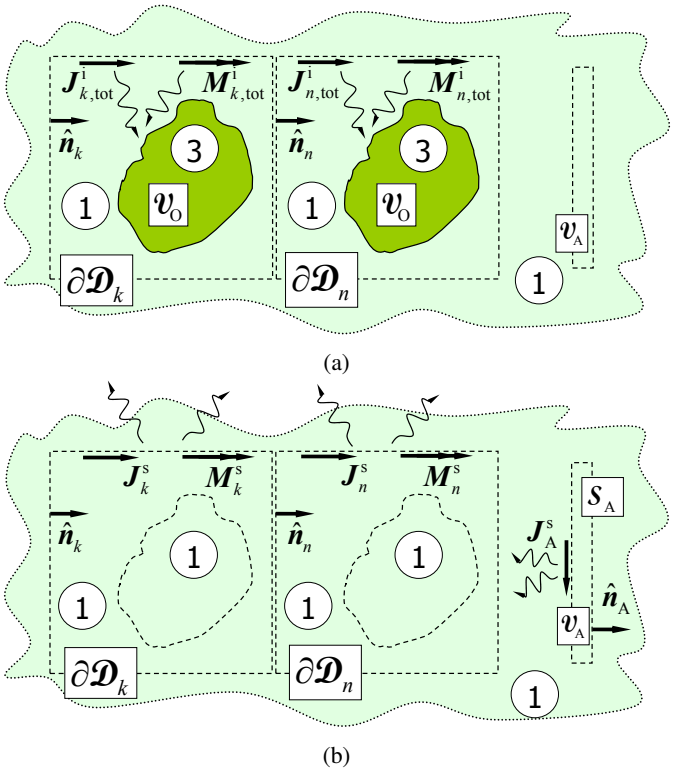

Fig. 2: Equivalent EM problems: (a) The SEP is *repeatedly* applied on a surface that tightly wraps one brick at a time (say, $\mathcal{D}_k$) so as to preserve equivalence inside that brick and to remove the antenna ($\mathcal{V}_\mathrm{A}$) as well as the remaining bricks ($\cup_{n\neq k}\mathcal{D}_n$); (b) The SEP is applied on a disjoint surface that tightly encloses all the bricks and the antenna so as to preserve equivalence outside the bricks and the antenna region, and to remove the antenna ($\mathcal{V}_\mathrm{A}$) and the bricks ($\cup_k \mathcal{D}_k$).

sake of simplicity we model the antenna excitation by means of the delta (or voltage) gap generator [67], [68]. As a result, since we set the voltage at each antenna port and we compute the current flowing therein, the natural network quantity, which can be obtained by solving the EM problem, is the admittance matrix.

We are now ready to apply LEGO to the EM problem of Fig. 1a. We start by enclosing the N_D anisotropic bodies in as many simple-shaped bricks $\mathcal{D}_k$, $k = 1, \ldots, N_D$, and we denote the boundary of $\mathcal{D}_k$ with $\partial\mathcal{D}_k$. The unit normal $\hat{\mathbf{n}}_k$ to $\partial\mathcal{D}_k$ is taken as pointing inwards $\mathcal{D}_k$ (Fig. 1b); correspondingly, the positive (negative) side of $\partial\mathcal{D}_k$ is indicated by $\partial\mathcal{D}_k^+$ ($\partial\mathcal{D}_k^-$). However, here the distinction between $\partial\mathcal{D}_k^+$ and $\partial\mathcal{D}_k^-$ is immaterial, since $\partial\mathcal{D}_k$ constitutes a mathematical separation surface [54] rather than a material interface (cf. [55]), and the EM properties of medium ① and ② are the same by hypothesis.

We suppose that $\mathcal{D}_k$ has been characterized by means of the scattering operator S_{kk}, whereas the multiple scattering among $\mathcal{D}_k$, $\mathcal{D}_n$, $n = 1, \ldots, N_D$, $n \neq k$ has been accounted for through the pair of transfer operators T_{kn} and T_{nk} [54]. To keep the exposition lucid, though, we postpone the derivation of S_{kk}, T_{kn}, and T_{nk} until Section III.

As we are concerned with a cluster of N_D identical bodies, all the scattering operators can be made equal to each other, provided we also consider bricks with the same shape, as we have argued in the Introduction. Nevertheless, the equations to be derived in the following are completely general, inasmuch as they depend neither on the shape nor on the content of $\mathcal{D}_k$.

B. Equivalent problems and unknown current densities

The theoretical framework for the definition of the EM bricks and the formulation of the EM problem of Fig. 1a is the Surface Equivalence Principle (SEP) [14], [69]. Thanks to the SEP, equivalent problems in a given region of space can be built as long as suitable surface electric ($\mathbf{J}$) and magnetic ($\mathbf{M}$) current densities are placed on the separation surface.

For instance, we invoke the SEP N_D times on $\partial\mathcal{D}_k$, $k = 1, \ldots, N_D$, as illustrated in Fig. 2a, in order to obtain N_D new problems that are equivalent to the original one inside $\mathcal{D}_k$, whereas the outside of $\mathcal{D}_k$ is the excluded region. With each step we end up introducing a set of equivalent *total incident* surface current densities, namely,

$$\mathbf{J}^\mathrm{i}_{k,\mathrm{tot}} \equiv \hat{\mathbf{n}}_k \times \mathbf{H}^\mathrm{i}_{k,\mathrm{tot}}, \tag{1a}$$

$$\mathbf{M}^\mathrm{i}_{k,\mathrm{tot}} \equiv \mathbf{E}^\mathrm{i}_{k,\mathrm{tot}} \times \hat{\mathbf{n}}_k, \tag{1b}$$

where $\mathbf{E}^\mathrm{i}_{k,\mathrm{tot}}$, $\mathbf{H}^\mathrm{i}_{k,\mathrm{tot}}$ represent the total (unknown) incident EM field on the boundary $\partial\mathcal{D}_k$, and $\hat{\mathbf{n}}_k$ is the inward pointing unit normal thereon. Moreover, the above currents radiate in the presence of the object inside $\mathcal{D}_k$ only, provided we "fill"

the excluded region with a material that has the same EM properties as those of medium ①.

A further application of the SEP, simultaneously on a disjoint surface comprised of the boundaries $\cup_{k=1}^{N_D}\partial\mathcal{D}_k$ *plus* the antenna surface $\mathcal{S}_\mathrm{A}$ (see Fig. 2b), allows us to define an equivalent problem in the region of space outside $\cup_{k=1}^{N_D}\mathcal{D}_k$ and $\mathcal{V}_\mathrm{A}$. In the process we introduce i) N_D sets of equivalent *scattered* surface current densities, viz.,

$$\mathbf{J}_k^\mathrm{s} \equiv -\hat{\mathbf{n}}_k \times \mathbf{H}_k^\mathrm{s}, \tag{2a}$$

$$\mathbf{M}_k^\mathrm{s} \equiv -\mathbf{E}_k^\mathrm{s} \times \hat{\mathbf{n}}_k, \tag{2b}$$

where $\mathbf{E}_k^\mathrm{s}$, $\mathbf{H}_k^\mathrm{s}$ is the (unknown) scattered EM field on $\partial\mathcal{D}_k$, and ii) the equivalent surface current densities

$$\mathbf{J}_\mathrm{A} \equiv \hat{\mathbf{n}}_\mathrm{A} \times \mathbf{H}_\mathrm{A}, \tag{3a}$$

$$\mathbf{M}_\mathrm{A} \equiv \mathbf{E}_\mathrm{A} \times \hat{\mathbf{n}}_\mathrm{A} = \mathbf{0}, \tag{3b}$$

where $\mathbf{E}_\mathrm{A}$, $\mathbf{H}_\mathrm{A}$ are the total electric and magnetic fields on the antenna surface $\mathcal{S}_\mathrm{A}$, and $\hat{\mathbf{n}}_\mathrm{A}$ denotes the unit normal thereon. Lastly, upon replacing the inside of the bricks and the conductors with a material endowed with parameters ε_1, μ_1, we are left with $\mathbf{J}_k^\mathrm{s}$, $\mathbf{M}_k^\mathrm{s}$, and $\mathbf{J}_\mathrm{A}$ radiating in a homogeneous unbounded medium.

We observe that $\mathbf{J}_{k,\mathrm{tot}}^\mathrm{i}$, $\mathbf{M}_{k,\mathrm{tot}}^\mathrm{i}$ (Fig. 2a) radiate the incident EM field due to all *external* sources towards the inside of $\mathcal{D}_k$. For the EM problem of Fig. 1b, such sources will be both (2a) and (2b) flowing on the boundaries of the remaining N_D-1 bricks and (3a) induced on the antenna conductors $\mathcal{S}_\mathrm{A}$ (Fig. 2b). Conversely, each pair $\mathbf{J}_k^\mathrm{s}$, $\mathbf{M}_k^\mathrm{s}$ produces the scattered EM fields that are actually radiated by secondary (polarization or magnetization) volume currents flowing in the region $\mathcal{V}_O$ occupied by the anisotropic object within $\mathcal{D}_k$.

C. LEGO equations for the bricks

The relationship between $\mathbf{J}_{k,\mathrm{tot}}^\mathrm{i}$, $\mathbf{M}_{k,\mathrm{tot}}^\mathrm{i}$ and $\mathbf{J}_k^\mathrm{s}$, $\mathbf{M}_k^\mathrm{s}$, just defined, is provided by the scattering operator S_{kk}, as follows:

$$q_k^\mathrm{s} = \mathsf{S}_{kk}\, q_{k,\mathrm{tot}}^\mathrm{i}, \quad \text{on } \partial\mathcal{D}_k, \tag{4}$$

where $q_{k,\mathrm{tot}}^\mathrm{i}$, q_k^s are the abstract 2×1 vectors

$$q_{k,\mathrm{tot}}^\mathrm{i} \equiv \begin{bmatrix} \sqrt{\eta_1}\mathbf{J}_{k,\mathrm{tot}}^\mathrm{i} \\ -\mathbf{M}_{k,\mathrm{tot}}^\mathrm{i}/\sqrt{\eta_1} \end{bmatrix}, \tag{5a}$$

$$q_k^\mathrm{s} \equiv \begin{bmatrix} \sqrt{\eta_1}\mathbf{J}_k^\mathrm{s} \\ -\mathbf{M}_k^\mathrm{s}/\sqrt{\eta_1} \end{bmatrix}, \tag{5b}$$

and $\eta_1 = \sqrt{\mu_1/\varepsilon_1}$ is the intrinsic impedance of medium ①. The latter normalization factor endows $q_{k,\mathrm{tot}}^\mathrm{i}$, q_k^s with the physical dimension of a power wave, i.e., $\mathrm{W}^{1/2}$/m. In light of (4), S_{kk} can be rightfully regarded as a generalization of the scattering matrix in network or waveguide theory [70], [71].

To proceed, we split the total equivalent incident currents into the contributions of the various sources, namely,

$$q_{k,\mathrm{tot}}^\mathrm{i} = q_k^\mathrm{i} + \sum_{\substack{n=1\\n\neq k}}^{N_D} q_{k(n)}^\mathrm{i}, \tag{6}$$

where q_k^i represents the equivalent incident currents due to $\mathbf{J}_\mathrm{A}$ on the antenna conductors, and the nth term of the summation constitutes the equivalent incident currents due to q_n^s flowing on the boundary of $\mathcal{D}_n$. The link between equivalent scattered currents on $\partial\mathcal{D}_n$ and additional incident currents $q_{k(n)}^\mathrm{i}$ on $\partial\mathcal{D}_k$ reads

$$q_{k(n)}^\mathrm{i} = \mathsf{T}_{kn} q_n^\mathrm{s}, \qquad \text{on } \partial\mathcal{D}_k, \qquad n\neq k, \tag{7}$$

where T_{kn} is the transfer operator between $\partial\mathcal{D}_n$ and $\partial\mathcal{D}_k$ (see Section III).

Next, upon substituting (7) into (6) and the latter into (4), and then *formally* solving for q_k^i and rearranging, we arrive at the set of N_D coupled functional equations

$$\mathsf{S}_{kk}^{-1} q_k^\mathrm{s} - \sum_{\substack{n=1\\n\neq k}}^{N_D} \mathsf{T}_{kn} q_n^\mathrm{s} = q_k^\mathrm{i}, \qquad k=1,\ldots,N_D, \tag{8}$$

which can be cast in a compact abstract matrix form as:

$$\mathsf{S}^{-1} q^\mathrm{s} = q^\mathrm{i}, \qquad \text{on } \partial\mathcal{D}_1 \cup \ldots \cup \partial\mathcal{D}_{N_D}, \tag{9}$$

where $q^{\mathrm{s,i}}$ are $N_D\times 1$ abstract vectors

$$q^{\mathrm{s,i}} \equiv \begin{bmatrix} q_1^{\mathrm{s,i}} \\ \vdots \\ q_{N_D}^{\mathrm{s,i}} \end{bmatrix}, \tag{10}$$

and

$$\mathsf{S}^{-1} \equiv \mathrm{diag}\{\mathsf{S}_{kk}^{-1}\} - \mathsf{T}, \tag{11}$$

is the total inverse scattering operator of the aggregate of the bricks [54]. Additionally, the total transfer operator T, an abstract $N_D\times N_D$ matrix, is defined as

$$\mathsf{T} \equiv \begin{bmatrix} 0 & -\mathsf{T}_{12} & \cdots & -\mathsf{T}_{1N_D} \\ -\mathsf{T}_{21} & 0 & \cdots & -\mathsf{T}_{2N_D} \\ \vdots & \vdots & \ddots & \vdots \\ -\mathsf{T}_{N_D1} & -\mathsf{T}_{N_D2} & \cdots & 0 \end{bmatrix}, \tag{12}$$

and, since $\mathsf{T}_{kn} \neq \mathsf{T}_{nk}$, it is not symmetric (Section III).

The total inverse scattering operator in (11) rigorously and elegantly captures the multiple scattering that occurs among the N_D anisotropic bodies. And yet, (11) is just a formal result, because first of all S_{kk} and its inverse cannot be obtained analytically for general geometries; secondly, S_{kk}^{-1} may not be defined at all when the scattering operator happens to be singular. Nevertheless, we shall show in Section V that the numerical solution of (9) is by no means critical, provided we apply the eigencurrents expansion and organize the calculations properly.

D. Electric field integral equation for the antenna

We now turn our attention to the antenna part of the EM problem. By enforcing the boundary condition (3b) for the total tangential electric field on $\mathcal{S}_\mathrm{A}$ we arrive at the electric field integral equation (EFIE)

$$\left[\mathbf{E}_\mathrm{A}^\mathrm{g} + \mathbf{E}_\mathrm{A}^\mathrm{s} + \sum_{k=1}^{N_D} \mathbf{E}_{\mathrm{A}k}^\mathrm{s}\right]_\mathrm{tan} = 0, \qquad \text{on } \mathcal{S}_\mathrm{A}, \tag{13}$$

where $\mathbf{E}^{\mathrm{g}}_{\mathrm{A}}$ is the impressed field supplemented by the external generator in the delta-gap approximation [67], [68], $\mathbf{E}^{\mathrm{s}}_{\mathrm{A}}$ is the secondary field produced by $\mathbf{J}_{\mathrm{A}}$ on $\mathcal{S}_{\mathrm{A}}$, and $\mathbf{E}^{\mathrm{s}}_{\mathrm{A}k}$ represents the field radiated by the scattered currents q^{s}_k on $\partial\mathcal{D}_k$. The subscript "tan" implies that (13) must hold true for the field components that are tangential to $\mathcal{S}_{\mathrm{A}}$.

Since the voltage gap generator [67] consists of the quasi-static approximation of the electric field existing at the open end of the coaxial cables connected to the antenna, $\mathbf{E}^{\mathrm{g}}_{\mathrm{A}}$ is effectively non-zero only at the antenna ports. In fact, the voltage gap model can be applied successfully as long as the actual antenna port is small as compared to *a*) the operational wavelength in the background medium and *b*) the antenna size. As an example, in the case of a single-port antenna

$$[\mathbf{E}^{\mathrm{g}}_{\mathrm{A}}]_{\tan} \equiv V_{\mathrm{G}}\hat{\boldsymbol{\nu}}\delta_{\gamma_A}, \qquad \text{on } \mathcal{S}_{\mathrm{A}}, \tag{14}$$

where V_{G} is the intensity of the voltage generator, γ_A is a line on $\mathcal{S}_{\mathrm{A}}$ that defines the antenna port, $\hat{\boldsymbol{\nu}}$ is a unit vector tangential to $\mathcal{S}_{\mathrm{A}}$ and locally perpendicular to γ_A, and δ_{γ_A} denotes a one-dimensional Dirac distribution on γ_A. Furthermore, in light of (14), there is no direct contribution from the generator onto the aggregate of bricks; this is reflected in the absence of a corresponding equivalent incident current in (9).

The tangential part of the electric field produced by $\mathbf{J}_{\mathrm{A}}$ on itself is given by

$$[\mathbf{E}^{\mathrm{s}}_{\mathrm{A}}]_{\tan} = \eta_1 \mathsf{L}_{\mathrm{ANT}}\mathbf{J}_{\mathrm{A}}, \qquad \text{on } \mathcal{S}_{\mathrm{A}}, \tag{15}$$

where

$$\begin{aligned}\mathsf{L}_{\mathrm{ANT}}\{\circ\} \equiv &-\mathrm{j}k_1 \int_{\mathcal{S}_{\mathrm{A}}} \mathrm{d}^2 r' G_1(R)\, \bar{\mathbf{I}}_{\mathrm{s}} \cdot \{\circ\} \\ &- \frac{\mathrm{j}\nabla_{\mathrm{s}}}{k_1} \int_{\mathcal{S}_{\mathrm{A}}} \mathrm{d}^2 r' G_1(R) \nabla'_{\mathrm{s}} \cdot \{\circ\}, \quad \mathbf{r} \in \mathcal{S}_{\mathrm{A}},\end{aligned} \tag{16}$$

is the standard EFIE operator [14]. Besides, $k_1 = \omega\sqrt{\varepsilon_1\mu_1}$ represents the wavenumber[1] in medium ①, $R = |\mathbf{r} - \mathbf{r}'|$ is the distance between field ($\mathbf{r}$) and source ($\mathbf{r}'$) points, and

$$G_1(R) \equiv \frac{\exp(-\mathrm{j}k_1 R)}{4\pi R}, \tag{17}$$

is the pertinent 3-D scalar Green function. Finally, $\bar{\mathbf{I}}_{\mathrm{s}} = \bar{\mathbf{I}} - \hat{\mathbf{n}}_{\mathrm{A}}\hat{\mathbf{n}}_{\mathrm{A}}$ is the surface unit dyadic tangential to $\mathcal{S}_{\mathrm{A}}$, $\nabla_{\mathrm{s}} = \bar{\mathbf{I}}_{\mathrm{s}} \cdot \nabla$, and $\nabla'_{\mathrm{s}} = -\nabla_{\mathrm{s}}$ means differentiation with respect to $\mathbf{r}'$.

E. Formulation with a modified EFIE

To finalize the formulation of the EM problem we need to include the multiple scattering phenomenon which occurs between the antenna and each one of the N_D bodies.

For instance, we observe that the antenna current $\mathbf{J}_A$ radiates the EM field $\mathbf{E}^{\mathrm{i}}_k$, $\mathbf{H}^{\mathrm{i}}_k$ on the boundary of $\mathcal{D}_k$. This can be written symbolically as

$$F^{\mathrm{i}}_{\mathrm{t}k} \equiv \begin{bmatrix} \mathbf{0} \\ \sqrt{\eta_1}\,\mathbf{H}^{\mathrm{i}}_{\mathrm{t}k} \end{bmatrix} = \sqrt{\eta_1}\,\mathsf{P}_{k\mathrm{A}}\mathbf{J}_{\mathrm{A}}, \tag{18}$$

where the surface integro-differential operator $\mathsf{P}_{k\mathrm{A}}$ is called the propagator from $\mathcal{S}_{\mathrm{A}}$ to $\partial\mathcal{D}_k$ (see Appendix A-C); besides, the subscript 't' stands for "tangential" to $\partial\mathcal{D}_k$. To convert the fields impinging on $\partial\mathcal{D}_k$ into the equivalent incident currents in (6), we resort to another propagator, as follows:

$$\mathsf{P}^{\mathrm{i}}_{kk}\, q^{\mathrm{i}}_k = F^{\mathrm{i}}_{\mathrm{t}k}, \qquad \text{on } \partial\mathcal{D}_k, \tag{19}$$

where $\mathsf{P}^{\mathrm{i}}_{kk}$ is a 2×2 abstract matrix of integro-differential operators on $\partial\mathcal{D}_k$, which is given explicitly in Appendix A-A.

Note that a null vector appears in the definition of $F^{\mathrm{i}}_{\mathrm{t}k}$ above, because the propagator $\mathsf{P}^{\mathrm{i}}_{kk}$ has been conveniently defined in such a way that only the incident magnetic field is required to produce the corresponding incident currents. Thanks to this expedient step followed, in the context of the numerical solution through the MoM and a symmetric inner product, the algebraic counterpart of $\mathsf{P}^{\mathrm{i}}_{kk}$ happens to be a symmetric matrix. It is also worthwhile mentioning that the calculation of q^{i}_k through (19) is preferable over the definition in terms of twisted tangential fields, namely,

$$\mathbf{J}^{\mathrm{i}}_k \equiv \hat{\mathbf{n}}_k \times \mathbf{H}^{\mathrm{i}}_k, \tag{20a}$$

$$\mathbf{M}^{\mathrm{i}}_k \equiv \mathbf{E}^{\mathrm{i}}_k \times \hat{\mathbf{n}}_k, \tag{20b}$$

since the latter equations are likely to yield less accurate results when evaluated numerically.

Now, solving (18) and (19) for q^{i}_k yields

$$q^{\mathrm{i}}_k = \sqrt{\eta_1}(\mathsf{P}^{\mathrm{i}}_{kk})^{-1}\mathsf{P}_{k\mathrm{A}}\mathbf{J}_{\mathrm{A}}, \quad \text{on } \partial\mathcal{D}_k, \tag{21}$$

which mathematically accounts for the interaction between the antenna and the brick $\mathcal{D}_k$.

The equivalent scattered currents q^{s}_k flowing on $\partial\mathcal{D}_k$ as a result of the presence of the body inside $\mathcal{D}_k$, in turn produce the EM fields $\mathbf{E}^{\mathrm{s}}_{\mathrm{A}k}$, $\mathbf{H}^{\mathrm{s}}_{\mathrm{A}k}$ on the antenna surface. Since only the electric field enters (13), we can express $\mathbf{E}^{\mathrm{s}}_{\mathrm{A}k}$ symbolically as

$$[\mathbf{E}^{\mathrm{s}}_{\mathrm{A}k}]_{\tan} = \sqrt{\eta_1}\,\mathsf{P}_{\mathrm{A}k}\, q^{\mathrm{s}}_k, \quad \text{on } \mathcal{S}_{\mathrm{A}}, \tag{22}$$

where the surface operator $\mathsf{P}_{\mathrm{A}k}$ is called the propagator from $\partial\mathcal{D}_k$ to the antenna, and it is a 1×2 abstract matrix of integro-differential operators on $\partial\mathcal{D}_k$, as detailed in Appendix A-C.

With the aid of (10) and (22) we can cast the combined contribution of the N_D bricks onto the antenna in a compact form as follows:

$$\sum_{k=1}^{N_D} [\mathbf{E}^{\mathrm{s}}_{\mathrm{A}k}]_{\tan} = \sqrt{\eta_1}\,\mathsf{P}_{\mathrm{AO}} q^{\mathrm{s}}, \quad \text{on } \mathcal{S}_{\mathrm{A}}, \tag{23}$$

where P_{AO} is a $1 \times N_D$ abstract matrix with entries

$$(\mathsf{P}_{\mathrm{AO}})_k = \mathsf{P}_{\mathrm{A}k}, \tag{24}$$

and q^{s} is given by (10). By inserting (21) into (9) and solving for q^{s} we obtain

$$q^{\mathrm{s}} = \sqrt{\eta_1}\,\mathsf{S}\mathsf{T}_{\mathrm{OA}}\mathbf{J}_{\mathrm{A}}, \quad \text{on } \partial\mathcal{D}_1 \cup \ldots \cup \partial\mathcal{D}_{N_D}, \tag{25}$$

where T_{OA} is an $N_D \times 1$ abstract matrix of operators with entries

$$(\mathsf{T}_{\mathrm{OA}})_k = (\mathsf{P}^{\mathrm{i}}_{kk})^{-1}\mathsf{P}_{k\mathrm{A}}. \tag{26}$$

[1]The wavenumber k_1 should not be confused with the brick index k.

Finally, inserting $q^{\rm s}$ as given by (25) into (23), and the result into (13), yields the modified EFIE for the current density $\mathbf{J}_{\rm A}$, viz.,

$$\eta_1 \left(\mathsf{L}_{\rm ANT} + \mathsf{L}_{\rm LEGO}\right) \mathbf{J}_{\rm A} = -[\mathbf{E}^{\rm g}_{\rm A}]_{\rm tan}, \quad \text{on } \mathcal{S}_{\rm A}, \tag{27}$$

where the operator

$$\mathsf{L}_{\rm LEGO} \equiv \mathsf{P}_{\rm AO}\mathsf{S}\mathsf{T}_{\rm OA}, \tag{28}$$

factors in the effect of the aggregate of bricks (and hence, of anisotropic bodies) on the antenna current $\mathbf{J}_{\rm A}$. In this regard, if we were able to cast $\mathsf{L}_{\rm ANT} + \mathsf{L}_{\rm LEGO}$ in the form of a radiation integral over $\mathcal{S}_{\rm A}$ and to single out the corresponding kernel explicitly, we would have obtained the Green's function relevant to the electric field produced by an elementary electric current density in the presence of the N_D objects.

The fact that (27) and (28) have exactly the same functional form as [61, Eq. (5)] — which were derived for antennas and a cluster of *isotropic* objects — is a welcome consequence of the modularity of LEGO. Indeed, it is evident that the assumption of anisotropic objects has an impact solely on the calculation of the scattering operators S_{kk}.

Once the antenna current density $\mathbf{J}_{\rm A}$ has been computed from (27), we can determine the equivalent scattered densities $q^{\rm s}$ from (25). Both $\mathbf{J}_{\rm A}$ and $q^{\rm s}$ contribute to the radiated EM field.

III. Scattering and transfer operators

In this section we derive explicit, though formal, expressions for S_{kk} and T_{kn}, T_{nk} in terms of suitable integral operators. We recall that in deriving S_{kk} we assume that media ① and ② possess the same EM properties. To gain more generality, we suppose that the object inside $\mathcal{D}_k$ has dyadic permittivity $\overline{\boldsymbol{\varepsilon}}_3$ and permeability $\overline{\boldsymbol{\mu}}_3$. Also, by invoking linearity and superposition we can work with a solitary brick $\mathcal{D}_k$ in medium ① illuminated by incident EM fields $\mathbf{E}^{\rm i}_k$, $\mathbf{H}^{\rm i}_k$, which are generated by some external source of radiation. In fact, we may as well assume that the equivalent incident currents $q^{\rm i}_k$ have been obtained by inverting (19).

To begin with, we observe that the EM field produced by $q^{\rm i}_k$ in the region $\mathcal{V}_{\rm O}$ occupied by the object inside $\mathcal{D}_k$ can be written formally as (Fig. 3a)

$$F^{\rm i}_{\rm o} \equiv \left[\begin{array}{c} \mathbf{D}^{\rm i}_{\rm o}/(\varepsilon_1\sqrt{\eta_1}) \\ \mathbf{B}^{\rm i}_{\rm o}\sqrt{\eta_1}/\mu_1 \end{array}\right] = \mathsf{P}_{ok}\, q^{\rm i}_k, \quad \text{in } \mathcal{V}_{\rm O}, \tag{29}$$

with $\mathbf{D}^{\rm i}_{\rm o}$, $\mathbf{B}^{\rm i}_{\rm o}$, the incident electric and magnetic flux densities within $\mathcal{V}_{\rm O}$. The propagator P_{ok} is a 2×2 matrix of dyadic surface operators whose kernel is the Green's function of media ① and ② (see Appendix A-B).

Next, we apply the Volume Equivalence Principle (VEP) and we replace the object with the equivalent electric and magnetic volume current densities (e.g., [22])

$$\begin{aligned} \mathbf{J}_{\rm o} &\equiv {\rm j}\,\omega[\,\bar{\mathbf{I}} - (\overline{\boldsymbol{\varepsilon}}_3(\mathbf{r})/\varepsilon_1)^{-1}]\cdot\mathbf{D}_{\rm o} \\ &= {\rm j}\,\omega\,\overline{\boldsymbol{\alpha}}_e(\mathbf{r})\cdot\mathbf{D}_{\rm o}, \qquad \mathbf{r}\in\mathcal{V}_{\rm O}, \end{aligned} \tag{30a}$$

$$\begin{aligned} \mathbf{M}_{\rm o} &\equiv {\rm j}\,\omega[\,\bar{\mathbf{I}} - (\overline{\boldsymbol{\mu}}_3(\mathbf{r})/\mu_1)^{-1}]\cdot\mathbf{B}_{\rm o} \\ &= {\rm j}\,\omega\,\overline{\boldsymbol{\alpha}}_h(\mathbf{r})\cdot\mathbf{B}_{\rm o}, \qquad \mathbf{r}\in\mathcal{V}_{\rm O}, \end{aligned} \tag{30b}$$

where $\overline{\boldsymbol{\alpha}}_e$ and $\overline{\boldsymbol{\alpha}}_h$ are the *contrast* dyadics, and $\mathbf{D}_{\rm o}$ and $\mathbf{B}_{\rm o}$ are the total electric and magnetic flux densities, respectively, within $\mathcal{V}_{\rm O}$. Accordingly, $\mathbf{D}_{\rm o}$, $\mathbf{B}_{\rm o}$ can be obtained from $F^{\rm i}_{\rm o}$ by solving the VIE (Fig. 3b)

$$\mathsf{X}_{\rm oo}\, q_{\rm o} = F^{\rm i}_{\rm o}, \qquad \text{in } \mathcal{V}_{\rm O}, \tag{31}$$

where

$$q_{\rm o} \equiv \left[\begin{array}{c} \mathbf{D}_{\rm o}/(\varepsilon_1\sqrt{\eta_1}) \\ \sqrt{\eta_1}\,\mathbf{B}_{\rm o}/\mu_1 \end{array}\right], \tag{32}$$

and $\mathsf{X}_{\rm oo}$ is a 2×2 matrix of volume operators over $\mathcal{V}_{\rm O}$ (see Appendix B). The volume currents $\mathbf{J}_{\rm o}$, $\mathbf{M}_{\rm o}$ in turn generate a scattered EM field on the $\partial\mathcal{D}_k$. The latter can be expressed mathematically in terms of $\mathbf{D}_{\rm o}$, $\mathbf{B}_{\rm o}$ as (Fig. 3c)

$$F^{\rm s}_{{\rm t}k} \equiv \left[\begin{array}{c} \mathbf{0} \\ \sqrt{\eta_1}\,\mathbf{H}^{\rm s}_{{\rm t}k} \end{array}\right] = \mathsf{P}_{k\,\rm o} q_{\rm o}, \quad \text{on } \partial\mathcal{D}_k, \tag{33}$$

where the propagator $\mathsf{P}_{k\,\rm o}$ is a 2×2 abstract matrix of dyadic volume operators involving the Green's function of media ① and ② (see Appendix A-B). The superscript 's' (short for "scattered") signifies that the fields in question propagate away from the object and out of the brick.

Eventually, a further application of the SEP over $\partial\mathcal{D}_k$ enables us to replace the scattered field $F^{\rm s}_{{\rm t}k}$ with equivalent scattered densities (Fig. 3d), as follows:

$$\mathsf{P}^{\rm s}_{kk}\, q^{\rm s}_k = F^{\rm s}_{{\rm t}k}, \quad \text{on } \partial\mathcal{D}_k, \tag{34}$$

where $q^{\rm s}_k$ is the abstract 2×1 vector introduced in (5b). The propagator $\mathsf{P}^{\rm s}_{kk}$ — which plays a similar role to $\mathsf{P}^{\rm i}_{kk}$ in (19) — is defined so as to require only the magnetic field $\mathbf{H}^{\rm s}_{{\rm t}k}$ to determine $q^{\rm s}_k$, and this accounts for the presence of the null vector in $F^{\rm s}_{{\rm t}k}$ in (33). In this way, as already observed for $\mathsf{P}^{\rm i}_{kk}$, the algebraic counterpart of $\mathsf{P}^{\rm s}_{kk}$ is also a symmetric matrix.

Now, by formally solving (29), (31), (33) and (34) for $q^{\rm s}_k$ as a function of $q^{\rm i}_k$ we find that[2]

$$q^{\rm s}_k = (\mathsf{P}^{\rm s}_{kk})^{-1}\mathsf{P}_{k\,\rm o}(\mathsf{X}_{\rm oo})^{-1}\mathsf{P}_{ok}\, q^{\rm i}_k = \mathsf{S}_{kk}\, q^{\rm i}_k, \tag{35}$$

which provides us with a suitable recipe for computing the scattering operator S_{kk}. The propagators $\mathsf{P}_{k\,\rm o}$, P_{ok} and the integral operator $\mathsf{X}_{\rm oo}$ are given in Appendices A-B, B for the special instances of either a dielectric body (with $\overline{\boldsymbol{\mu}}_3 = \mu_1\bar{\mathbf{I}}$) or a magnetic one (with $\overline{\boldsymbol{\varepsilon}}_3 = \varepsilon_1\bar{\mathbf{I}}$).

The interaction between bricks $\mathcal{D}_k$, $\mathcal{D}_n$ can be obtained as follows. In a similar fashion to (19), we turn the incident fields onto $\partial\mathcal{D}_k$ (or $\partial\mathcal{D}_n$) into equivalent surface current densities $q^{\rm i}_{k(n)}$ (or $q^{\rm i}_{n(k)}$). Symbolically, we write

$$\mathsf{P}^{\rm i}_{kk}\, q^{\rm i}_{k(n)} = \mathsf{P}_{kn}\, q^{\rm s}_n, \quad \text{on } \partial\mathcal{D}_k, \qquad n\neq k, \tag{36a}$$

$$\mathsf{P}^{\rm i}_{nn}\, q^{\rm i}_{n(k)} = \mathsf{P}_{nk}\, q^{\rm s}_k, \quad \text{on } \partial\mathcal{D}_n, \qquad k\neq n, \tag{36b}$$

where the propagators $\mathsf{P}^{\rm i}_{kk}$, $\mathsf{P}^{\rm i}_{nn}$ are the same as in (19). Besides, the propagators P_{kn}, P_{nk} (given in Appendix A-A) are 2×2 abstract matrices whose non-null entries are dyadic

[2]This expression for S_{kk} differs from the one in [54, Eq. (11)] for a minus sign, which is due to different definitions adopted for the operator $\mathsf{X}_{\rm oo}$.

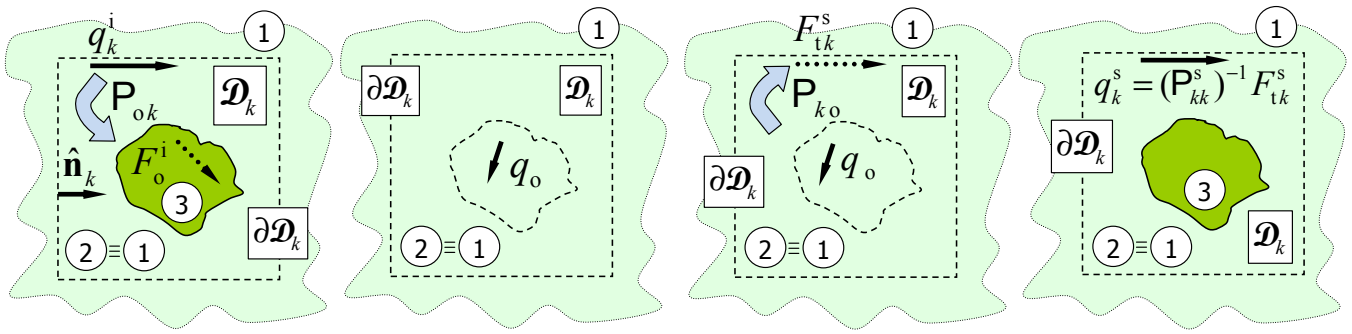

Fig. 3: Derivation of the scattering operator of $\mathcal{D}_k$ in the case when host (②) and background (①) medium have the same EM properties: (a) The equivalent incident currents q^{i}_k on $\partial\mathcal{D}_k$ produce incident fields $F^{\mathrm{i}}_{\mathrm{o}}$ in the region occupied by the object; (b) The object "reacts" with polarization and/or magnetization currents q_{o}; (c) The currents q_{o} produce scattered fields $F^{\mathrm{s}}_{\mathrm{t}k}$ on $\partial\mathcal{D}_k$; (d) The scattered fields are replaced with equivalent scattered currents q^{s}_k.

integro-differential operators. The formal inversion of (36a), (36b) yields

$$q^{\mathrm{i}}_{k(n)} = (\mathsf{P}^{\mathrm{i}}_{kk})^{-1}\mathsf{P}_{kn}\, q^{\mathrm{s}}_n = \mathsf{T}_{kn}\, q^{\mathrm{s}}_n, \qquad n \neq k, \tag{37a}$$

$$q^{\mathrm{i}}_{n(k)} = (\mathsf{P}^{\mathrm{i}}_{nn})^{-1}\mathsf{P}_{nk}\, q^{\mathrm{s}}_k = \mathsf{T}_{nk}\, q^{\mathrm{s}}_k, \qquad k \neq n, \tag{37b}$$

where the dimensionless *transfer* operators T_{kn}, T_{nk} map scattered currents on $\partial\mathcal{D}_{n,k}$ onto incident currents on $\partial\mathcal{D}_{k,n}$.

The propagators involved in (37a) and (37b) depend solely on the shape of a brick. Therefore, regardless of the content of a brick, if $\mathcal{D}_k$ and $\mathcal{D}_n$ have the same shape, then $\mathsf{P}^{\mathrm{i}}_{kk} = \mathsf{P}^{\mathrm{i}}_{nn}$, hence, we need only compute either one. By contrast, even in the case when $\partial\mathcal{D}_k = \partial\mathcal{D}_n$, it turns out that $\mathsf{P}_{kn} \neq \mathsf{P}_{nk}$. For these reasons — but also because $\mathsf{P}^{\mathrm{i}}_{kk}$ and $\mathsf{P}^{\mathrm{i}}_{nn}$ do not commute with P_{kn} and P_{nk} — no simple relationship exists between T_{kn} and T_{nk}, and the total transfer operator T in (12) is not symmetric, as we anticipated. It can be shown that the algebraic counterparts of the non-null entries of P_{kn} and P_{nk} (see Appendix A-A) are transposes of each other, provided the MoM is implemented by using a symmetric inner product.

IV. Numerical solution with Moments Method

We now describe the application of the baseline Method of Moments (MoM) in the Galerkin's form [14] for the calculation of scattering and transfer operators in (35) and (37a), (37b), the object-to-antenna propagators (24) and the antenna-to-object transfer operators (26). Furthermore, we derive a weak form corresponding to (25) and (27).

We begin by modelling the surface of the bricks and the conducting elements with 3-D triangular tessellations, and the anisotropic objects with tetrahedral meshes. Then, we express the surface electric and magnetic current densities flowing on the boundary of a brick as [54]

$$q^{\mathrm{i}}_k = \sum_{p=1}^{N_F} \begin{bmatrix} \mathbf{f}_{kp}(\mathbf{r})\sqrt{\eta_1}J^{\mathrm{i}}_{kp} \\ -\mathbf{g}_{kp}(\mathbf{r})M^{\mathrm{i}}_{kp}/\sqrt{\eta_1} \end{bmatrix}, \quad \mathbf{r} \in \partial\mathcal{D}_k, \tag{38a}$$

$$q^{\mathrm{s}}_k = \sum_{p=1}^{N_F} \begin{bmatrix} \mathbf{f}_{kp}(\mathbf{r})\sqrt{\eta_1}J^{\mathrm{s}}_{kp} \\ -\mathbf{g}_{kp}(\mathbf{r})M^{\mathrm{s}}_{kp}/\sqrt{\eta_1} \end{bmatrix}, \quad \mathbf{r} \in \partial\mathcal{D}_k, \tag{38b}$$

where $\{\mathbf{f}_{kp}(\mathbf{r})\}_{p=1}^{N_F}$ and $\{\mathbf{g}_{kp}(\mathbf{r})\}_{p=1}^{N_F}$ constitute two sets of N_F sub-sectional real divergence-conforming surface vector basis functions [72] associated with all the edges of the underlying 3-D triangular-facet mesh. Here, we choose $\mathbf{f}_{kp} = \mathbf{g}_{kp}$, although the functions used to express the electric and magnetic current densities need not be the same.

Likewise, we expand the flux densities within an anisotropic body as [62]

$$q_{\mathrm{o}} = \sum_{m=1}^{N_O} \begin{bmatrix} \mathbf{v}_m(\mathbf{r})D_m/(\varepsilon_1\sqrt{\eta_1}) \\ \mathbf{v}_m(\mathbf{r})\sqrt{\eta_1}B_m/\mu_1 \end{bmatrix}, \quad \mathbf{r} \in \mathcal{V}_{\mathrm{O}}, \tag{39}$$

where $\{\mathbf{v}_m(\mathbf{r})\}_{m=1}^{N_O}$ represents a set of N_O sub-sectional real divergence-conforming volume vector basis functions [73]. In particular, if the body is either electric or magnetic, (39) will reduce to an expansion for just $\mathbf{D}_{\mathrm{o}}$ or $\mathbf{B}_{\mathrm{o}}$, respectively (see Appendices A-B and B). To account for the fact that the normal components of $\mathbf{D}_{\mathrm{o}}$ and $\mathbf{B}_{\mathrm{o}}$ do not vanish on the boundary $\partial\mathcal{V}_{\mathrm{O}}$ of the object, the functions $\mathbf{v}_m$ are to be associated with *all* the triangular facets of the tetrahedral mesh.

Finally, we express $\mathbf{J}_{\mathrm{A}}$ on $\mathcal{S}_{\mathrm{A}}$ as [61]

$$\mathbf{J}_{\mathrm{A}}(\mathbf{r}) = \sum_{l=1}^{N_A} \mathbf{h}_l(\mathbf{r})I_l, \quad \mathbf{r} \in \mathcal{S}_{\mathrm{A}}, \tag{40}$$

where $\{\mathbf{h}_l(\mathbf{r})\}_{l=1}^{N_A}$ are N_A real divergence-conforming surface vector basis functions [72] associated with the *inner* edges of the relevant triangular tessellation.

To finalize the application of the MoM we also need three L^2 symmetric inner products defined as

$$(\mathbf{a},\mathbf{F})_{\partial\mathcal{D}_k} \equiv \int_{\partial\mathcal{D}_k} \mathrm{d}^2r\, \mathbf{a}\cdot\mathbf{F}, \quad \mathbf{a} \in \{\mathbf{f}_{kp},\mathbf{g}_{kp}\}_{p=1}^{N_F}, \tag{41a}$$

$$(\mathbf{a},\mathbf{F})_{\mathcal{V}_{\mathrm{O}}} \equiv \int_{\mathcal{V}_{\mathrm{O}}} \mathrm{d}^3r\, \mathbf{a}\cdot\mathbf{F}, \quad \mathbf{a} \in \{\mathbf{v}_m\}_{m=1}^{N_O}, \tag{41b}$$

$$(\mathbf{a},\mathbf{F})_{\mathcal{S}_{\mathrm{A}}} \equiv \int_{\mathcal{S}_{\mathrm{A}}} \mathrm{d}^2r\, \mathbf{a}\cdot\mathbf{F}, \quad \mathbf{a} \in \{\mathbf{h}_l\}_{l=1}^{N_A}, \tag{41c}$$

with $\mathbf{F}$ a complex vector field in $\partial\mathcal{D}_k$, $\mathcal{V}_{\mathrm{O}}$ and $\mathcal{S}_{\mathrm{A}}$, in (41a), (41b) and (41c), respectively.

For ease of manipulation, it is convenient to collect the expansion coefficients in (38a), (38b), (39) and (40) into column vectors $[q_k^{\mathrm{i}}]$, $[q_k^{\mathrm{s}}]$, $[q_{\mathrm{o}}]$, $[J_{\mathrm{A}}]$, as follows

$$[q_k^{\mathrm{s,i}}] = \begin{bmatrix} J_{k1}^{\mathrm{s,i}}\sqrt{\eta_1} \\ \vdots \\ J_{kN_F}^{\mathrm{s,i}}\sqrt{\eta_1} \\ -M_{k1}^{\mathrm{s,i}}/\sqrt{\eta_1} \\ \vdots \\ -M_{kN_F}^{\mathrm{s,i}}/\sqrt{\eta_1} \end{bmatrix}, \quad [q_{\mathrm{o}}] = \begin{bmatrix} D_1/(\varepsilon_1\sqrt{\eta_1}) \\ \vdots \\ D_{N_O}/(\varepsilon_1\sqrt{\eta_1}) \\ \sqrt{\eta_1}B_1/\mu_1 \\ \vdots \\ \sqrt{\eta_1}B_{N_O}/\mu_1 \end{bmatrix}, \quad (42)$$

$$[J_{\mathrm{A}}] = \begin{bmatrix} I_1 \\ \vdots \\ I_{N_A} \end{bmatrix}. \quad (43)$$

Following the manipulations above, we proceed to determine the weak form of equations and operators.

For instance, we insert (38a) into (29), (39) into (31), and we project them onto $\mathcal{V}_{\mathrm{O}}$ with (41b); then, we insert (38b) into (34), and we project it onto $\partial\mathcal{D}_k$ with (41a). Upon solving the trio of resulting equations for $[q_k^{\mathrm{s}}]$ in terms of $[q_k^{\mathrm{i}}]$, we arrive at the expression for the algebraic scattering operator

$$[S_{kk}] = [P_{kk}^{\mathrm{s}}]^{-1}\,[P_{\mathrm{ko}}]\,[X_{\mathrm{oo}}]^{-1}\,[P_{\mathrm{ok}}]\,, \quad (44)$$

where with transparent notation each matrix represents the algebraic counterpart of the corresponding integral operator in (35). As regards the size of the matrices in (44), $[P_{kk}^{\mathrm{s}}]$ is $2N_F \times 2N_F$, $[X_{\mathrm{oo}}]$ is $2N_O \times 2N_O$, and $[P_{\mathrm{ko}}]$, $[P_{\mathrm{ok}}]$ are $2N_F \times 2N_O$, $2N_O \times 2N_F$, respectively. However, if the object within $\mathcal{D}_k$ is either electric or magnetic, then $[X_{\mathrm{oo}}]$ is $N_O \times N_O$, and $[P_{\mathrm{ko}}]$, $[P_{\mathrm{ok}}]$ are $2N_F \times N_O$, $N_O \times 2N_F$, because either $\mathbf{M}_{\mathrm{o}}$ or $\mathbf{J}_{\mathrm{o}}$ is zero in $\mathcal{V}_{\mathrm{O}}$.

By inserting (38b) and a similar expansion for $q_{k(n)}^{\mathrm{i}}$ into (36a), projecting onto $\partial\mathcal{D}_k$ with (41a), and formally solving for $[q_k^{\mathrm{s}}]$ versus $[q_{k(n)}^{\mathrm{i}}]$, we can express the algebraic transfer operator as

$$[T_{kn}] = [P_{kk}^{\mathrm{i}}]^{-1}\left[P_{kn}^{\mathrm{i}}\right], \quad (45)$$

where both matrices are $2N_F \times 2N_F$; the expression for $[T_{nk}]$ ensues from (45) by swapping the indices n, k.

By substituting (38a) into (19) and (40) into (18), projecting onto $\partial\mathcal{D}_k$ with (41a), and solving for $[q_k^{\mathrm{i}}]$ with respect to $[J_{\mathrm{A}}]$ we get

$$[T_{\mathrm{OA}k}] = [P_{kk}^{\mathrm{i}}]^{-1}\,[P_{k\mathrm{A}}]\,, \quad (46)$$

where $[P_{k\mathrm{A}}]$ is size $2N_F \times N_A$. Similarly, inserting (38b) into (22) and projecting onto $\mathcal{S}_{\mathrm{A}}$ with (41c) yields $[P_{\mathrm{A}k}]$, whose size is $N_A \times 2N_F$. The matrices $[T_{\mathrm{OA}k}]$ and $[P_{\mathrm{A}k}]$ are needed to form $[L_{\mathrm{LEGO}}]$, the algebraic counterpart of (28).

By inserting (40) into (15), and projecting onto $\mathcal{S}_{\mathrm{A}}$ with (41c), we obtain $[L_{\mathrm{ANT}}]$, the algebraic counterpart of the EFIE operator (16). More specifically, the source term corresponding with (14) and the right-hand side of (27) is a column vector $[E_{\mathrm{A}}^{\mathrm{g}}]$ with N_A entries given by

$$\begin{aligned} E_{\mathrm{A}l}^{\mathrm{g}} &= \int_{\mathcal{S}_{\mathrm{A}}} \mathrm{d}^2 r\, \mathbf{h}_l(\mathbf{r}) \cdot \mathbf{E}_{\mathrm{A}}^{\mathrm{g}}(\mathbf{r}) \\ &= V_{\mathrm{G}} \int_{\gamma_{\mathrm{A}}} \mathrm{d}r\, \mathbf{h}_l(\mathbf{r}) \cdot \hat{\boldsymbol{\nu}}, \end{aligned} \quad (47)$$

which, as a result of the delta-gap generator model (14), are non-null only for those test functions among $\mathbf{h}_l(\mathbf{r})$ that are associated with the inner edges spanning the line γ_{A} in the triangular-facet mesh of $\mathcal{S}_{\mathrm{A}}$.

Now, by making use of (44) and (45) the algebraic total inverse scattering operator (of size $2N_FN_D \times 2N_FN_D$) can be written as

$$[S]^{-1} = \begin{bmatrix} [S_{11}]^{-1} & -[T_{12}] & \cdots & -[T_{1N_D}] \\ -[T_{21}] & [S_{22}]^{-1} & \cdots & -[T_{2N_D}] \\ \vdots & \vdots & \ddots & \vdots \\ -[T_{N_D1}] & -[T_{N_D2}] & \cdots & [S_{N_DN_D}]^{-1} \end{bmatrix}, \quad (48)$$

whereas the algebraic equivalent of the LEGO operator (28) reads

$$[L_{\mathrm{LEGO}}] = [P_{\mathrm{AO}}]\,[S]\,[T_{\mathrm{OA}}]\,, \quad (49)$$

with

$$[P_{\mathrm{AO}}] = \left[[P_{\mathrm{A}1}] \cdots [P_{\mathrm{A}N_D}]\right], \quad (50)$$

$$[T_{\mathrm{OA}}] = \begin{bmatrix} [T_{\mathrm{OA}1}] \\ \vdots \\ [T_{\mathrm{OA}N_D}] \end{bmatrix}, \quad (51)$$

and $[S]$ is the inverse of $[S]^{-1}$.

Lastly, in light of (47), (49), (50) and (51), the weak form of (25), (27) reads

$$[q^{\mathrm{s}}] = \sqrt{\eta_1}\,[S]\,[T_{\mathrm{OA}}]\,[J_{\mathrm{A}}]\,, \quad (52)$$

$$\eta_1([L_{\mathrm{ANT}}] + [L_{\mathrm{LEGO}}])\,[J_{\mathrm{A}}] = -\,[E_{\mathrm{A}}^{\mathrm{g}}]\,, \quad (53)$$

where $[q^{\mathrm{s}}]$ is a column vector with N_D block entries $[q_k^{\mathrm{s}}]$ as defined in (42).

As long as the number N_A of basis functions $\mathbf{h}_l(\mathbf{r})$ is not too large, we can solve the system (53) (of rank N_A) by means of direct solvers, such as the LU factorization [65]. The real challenge, though, is posed by the very determination of the LEGO matrix $[L_{\mathrm{LEGO}}]$, because that computation entails an inversion of $[S]^{-1}$ in (48), as can be gleaned from (49). In fact, even if we suppose the scattering matrices $[S_{kk}]$ are invertible so that $[S]^{-1}$ can actually be built explicitly, $[S]^{-1}$ may already become a large matrix, even for a moderate number N_D of EM bricks in the model. Worse still, if $[S_{kk}]$ is singular, then the representation (48) — being just formal — cannot be used to determine $[S]$ in the first place. These considerations also apply to (52) which we need to retrieve the coefficients of the scattered currents on $\cup_{k=1}^{N_D}\partial\mathcal{D}_k$. Thus, to cope with the occurrence of a large and possibly undefined matrix $[S]^{-1}$, we adopt the eigencurrents expansion method (EEM).

V. Eigencurrents expansion and compression

The application of the eigencurrents expansion method (EEM) to the solution of the LEGO equation (9) alone was extensively described in [54], [66]. Here, we follow the same strategy to compute the matrix product $[S]\,[T_{\rm OA}]$, which enters the algebraic LEGO operator (49) and the expression of the scattered currents coefficients $[q^{\rm s}]$ in (52). Therefore, the main goal is the efficient and stable calculation of $[S]$.

To begin, we consider the matrix of $2N_F$ eigenvectors $[V_{kk}]$ of the algebraic scattering operator (44) defined through

$$[S_{kk}]\,[V_{kk}] = [V_{kk}]\,\mathrm{diag}\{\lambda_q^{(k)}\}, \tag{54}$$

where $\lambda_q^{(k)}$, $q = 1, \ldots, 2N_F$, denote the eigenvalues of $[S_{kk}]$. We also assume that the eigenvalues are sorted in descending order, i.e., $|\lambda_q^{(k)}| \geq |\lambda_{q+1}^{(k)}|$, and that this ordering is reflected on the columns of $[V_{kk}]$ in an obvious way. Upon combining the $2N_F$ elements of each eigenvector with the basis functions $\mathbf{f}_{kp}$, $\mathbf{g}_{kp}$, as is prescribed by (38a), we obtain on $\partial\mathcal{D}_k$ a set of surface current densities which we refer to as the *eigencurrents* of $\mathcal{D}_k$, in light of (54) and the role played by $[S_{kk}]$.

In the eigencurrents expansion method (EEM) we employ the eigencurrents as local entire-domain basis functions on $\partial\mathcal{D}_k$. The desired compression of $[S]^{-1}$ is then achieved because only the eigencurrents associated with the larger eigenvalues $\lambda_q^{(k)}$ (usually only a few) must be retained to expand the currents on $\partial\mathcal{D}_k$.

This is accomplished by first expressing $[S]^{-1}$ in the basis of the eigenvectors of $[S_{kk}]$, as follows:

$$[\tilde{S}]^{-1} = [V]^{-1}\,[S]^{-1}\,[V]\,, \tag{55}$$

where $[V]$ is a block-diagonal matrix with N_D diagonal blocks given by $[V_{kk}]$. More specifically, in view of (48) and (54), we can write

$$([\tilde{S}]^{-1})_{kn} = \begin{cases} \mathrm{diag}\{1/\lambda_q^{(k)}\}, & k = n, \\ -\,[V_{kk}]^{-1}\,[T_{kn}]\,[V_{nn}]\,, & k \neq n. \end{cases} \tag{56}$$

Now, $[\tilde{S}]^{-1}$ would be an exactly diagonal matrix, if we had used its *true* eigenvectors, but the latter are just the quantities we cannot compute either because $[\tilde{S}]^{-1}$ is too large, or because $[S_{kk}]$ is singular, or both. As it turns out, though, most of the entries of (55) are relatively small and can be safely set to zero.

To this purpose, we observe that the eigencurrents of $\mathcal{D}_k$ can be separated into two complementary sub-sets: *coupled* and *uncoupled*. The former — corresponding with the larger eigenvalues $\lambda_q^{(k)}$, $q = 1, \ldots, N_C$ — produce substantial radiation, and hence they contribute to the multiple scattering that takes place among the bricks. On the contrary, the uncoupled eigencurrents — associated with the smaller and possibly null eigenvalues $\lambda_q^{(k)}$, $q = N_C + 1, \ldots, 2N_F$ — generate scattered fields that remain mostly confined around $\mathcal{D}_k$; hence, they are only necessary to describe the scattered currents on the very same brick.

To proceed with the inversion of $[\tilde{S}]^{-1}$ we rearrange rows and columns as follows:

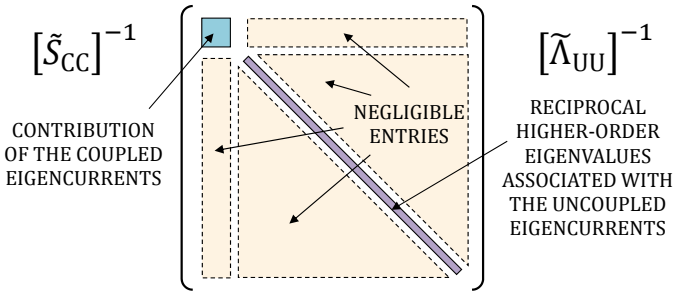

Fig. 4: To illustrate the partition and subsequent compression of the total inverse scattering operator $[S]^{-1}$ in the basis of the eigencurrents.

1) The entries relevant to two coupled eigencurrents are shifted to the upper left corner of the matrix;
2) The entries corresponding with two uncoupled eigencurrents are displaced to the lower right corner of the matrix;
3) The entries pertinent to a pair of coupled and uncoupled eigencurrents are moved either to the upper right part or to the lower left part of the matrix.

Symbolically, we can write

$$[\hat{S}]^{-1} = [P]^T\,[\tilde{S}]^{-1}\,[P] = \begin{bmatrix} [\tilde{S}_{\rm CC}]^{-1} & [\tilde{S}_{\rm CU}]^{-1} \\ [\tilde{S}_{\rm UC}]^{-1} & [\tilde{S}_{\rm UU}]^{-1} \end{bmatrix}, \tag{57}$$

where the subscript 'C' ('U') stands for coupled (uncoupled) and $[P]$ represents a suitable $2N_FN_D \times 2N_FN_D$ permutation matrix [65]. In accordance with the notion of coupled-uncoupled eigencurrents we observe that:

1) the matrix $[\tilde{S}_{\rm CC}]^{-1}$ is dominant;
2) the off-diagonal matrices $[\tilde{S}_{\rm CU}]^{-1}$ and $[\tilde{S}_{\rm UC}]^{-1}$ must be relatively small;
3) the off-diagonal entries of $[\tilde{S}_{\rm UU}]^{-1}$ must be relatively small or null.

Based on these observations, we approximate (57) as

$$[\hat{S}]^{-1} \approx \begin{bmatrix} [\tilde{S}_{\rm CC}]^{-1} & [0] \\ [0] & [\tilde{\Lambda}_{\rm UU}]^{-1} \end{bmatrix}, \tag{58}$$

with $[\tilde{\Lambda}_{\rm UU}]$ representing a diagonal matrix that contains all the eigenvalues associated with the uncoupled eigencurrents; the reduction process is graphically illustrated in Fig. 4. In this way, the calculation of $[S]$ has been reduced to the separate inversion of $[\tilde{S}_{\rm CC}]^{-1}$ and $[\tilde{\Lambda}_{\rm UU}]^{-1}$.

The matrix $[\tilde{S}_{\rm CC}]^{-1}$ has the rank N_CN_D, which is relatively small as compared to the rank of the original uncompressed inverse scattering operator (48); thus, we can obtain $[\tilde{S}_{\rm CC}]$ with the LU factorization [65]. Besides, the diagonal of $[\tilde{S}_{\rm CC}]^{-1}$ is comprised of the reciprocal eigenvalues germane to the coupled eigencurrents, as is evident from (56). Since these eigenvalues are relatively large — although $|\lambda_q^{(k)}| \leq 1$ — their numerical inversion is stable, and hence, $[\tilde{S}_{\rm CC}]^{-1}$ is well defined. In addition, we need not build $[\tilde{\Lambda}_{\rm UU}]^{-1}$ at all, since from (55) we already know the eigenvalues of $[S_{kk}]$. Therefore, the occurrence of very small or possibly null eigenvalues does not pose any numerical issue.

To determine the algebraic LEGO operator (49) we first express the matrices $[P_{\rm AO}]$ and $[T_{\rm OA}]$ in the basis of eigenvectors of $[S_{kk}]$ as well and then shuffle the entries thereof with the permutation matrix $[P]$. The result reads

$$\begin{aligned}[L_{\rm LEGO}] &= \\ &= [P_{\rm AO}]\,[V]\,[P]\,[\hat{S}]\,[P]^T\,[V]^{-1}\,[T_{\rm OA}] \\ &= \left[[\tilde{P}_{\rm AO,C}] \quad [\tilde{P}_{\rm AO,U}]\right][\hat{S}]\begin{bmatrix}[\tilde{T}_{\rm OA,C}]\\ [\tilde{T}_{\rm OA,U}]\end{bmatrix} \\ &\approx [\tilde{P}_{\rm AO,C}][\tilde{S}_{\rm CC}][\tilde{T}_{\rm OA,C}] + [\tilde{P}_{\rm AO,U}][\tilde{\Lambda}_{\rm UU}][\tilde{T}_{\rm OA,U}], \quad (59)\end{aligned}$$

where we have made use of (58) in computing $[\hat{S}]$. The second contribution in the rightmost r.h.s. of (59) can be neglected altogether, because the uncoupled eigenvalues are relatively small. From a physical standpoint, the latter implies that the uncoupled eigencurrents generate fields that do not propagate towards the antenna.

For the calculation of $[q^{\rm s}]$ in (52) we proceed in a similar fashion, namely,

$$\begin{aligned}[q^{\rm s}] &= \sqrt{\eta_1}\,[V]\,[P]\,[\hat{S}]\,[P]^T\,[V]^{-1}\,[T_{\rm OA}]\,[J_{\rm A}] \\ &= \sqrt{\eta_1}\,[V]\,[P]\,[\hat{S}]\begin{bmatrix}[\tilde{T}_{\rm OA,C}]\\ [\tilde{T}_{\rm OA,U}]\end{bmatrix}[J_{\rm A}] \\ &\approx \sqrt{\eta_1}\,[V]\,[P]\begin{bmatrix}[\tilde{S}_{\rm CC}][\tilde{T}_{\rm OA,C}]\\ [\tilde{\Lambda}_{\rm UU}][\tilde{T}_{\rm OA,U}]\end{bmatrix}[J_{\rm A}]\,, \quad (60)\end{aligned}$$

where again the matrix $[\tilde{\Lambda}_{\rm UU}][\tilde{T}_{\rm OA,U}]$ can be neglected.

If all the scattering operators are equal to each other, then we have to perform the spectral decomposition (54) and the formal inversion of $[V_{kk}]$ only once. Besides, the total number of coupled eigencurrents will be $N_C N_D$, which is the size of $[\tilde{S}_{\rm CC}]^{-1}$, the only matrix we really have to invert to compute $[L_{\rm LEGO}]$ and, at a later stage, the scattered current coefficients $[q^{\rm s}]$.

We conclude this section by observing that, from a computational viewpoint, it is desirable to use as few eigencurrents as possible, so as to keep the size $N_C N_D$ of $[\tilde{S}_{\rm CC}]^{-1}$ at bay. Obviously, the number of coupled eigencurrents cannot in any case exceed the total number of basis functions $2N_F$ introduced on $\partial\mathcal{D}_k$ to expand the equivalent current densities thereon. Furthermore, the very form of (44) suggests that $[S_{kk}]$ may be rank deficient, if the size of $[X_{\rm oo}]$ is smaller than the size of $[P^{\rm s}_{kk}]$. Therefore, the maximum number of coupled eigencurrents is

$$N_{C,\max} = \min\{2N_F, 2N_O\}, \quad (61)$$

if the embedded object is both magnetic and dielectric or else,

$$N_{C,\max} = \min\{2N_F, N_O\}, \quad (62)$$

if the object is either magnetic or dielectric [see (39)].

VI. Validation and Convergence

The solution of (25) and (27), which is based on the weak form (52) and (53), has been implemented in an extended numerical code. In this section we consider the validation of the hybrid LEGO-EFIE approach, and we discuss the convergence of the solution with the number coupled eigencurrents retained for the inversion of (57).

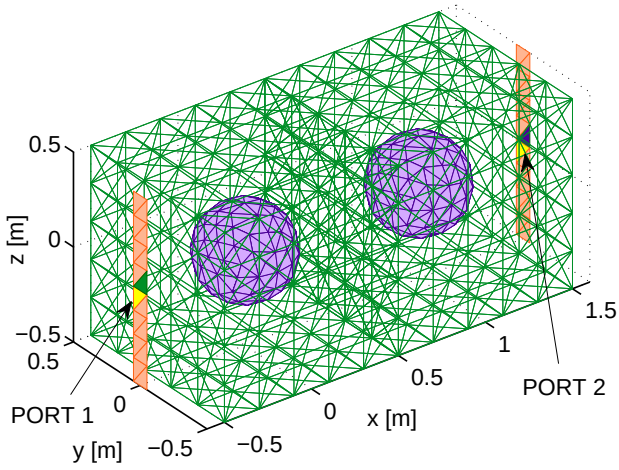

Fig. 5: For testing LEGO-EFIE: surface and volume meshes of two strip-dipoles and two dielectric spheres embedded in as many cubic bricks. *Data*: radius of spheres 25 cm, width of dipoles 10 cm, height of dipoles (d) and edge of bricks 100 cm, separation of dipoles 220 cm. (After [57].)

A. Example of validation

We examine the simple antenna problem of Fig. 5 in which two strip-dipole antennas are symmetrically placed across two dielectric spheres (medium ③) from each other.

The antenna-objects system is immersed in free space (medium ① and ② have the same EM parameters), in accordance with the general setup sketched in Fig. 1. To model the problem with LEGO we embed each sphere inside a cubic brick; the center of the sphere coincides with that of the surrounding brick (see the caption of Fig. 5 for geometrical data). The number of basis functions on the dipoles, on the surface of each brick and in each sphere are $N_A = 15 \times 2 = 30$, $2N_F = 1800$ and $N_O = 1834$, respectively.

To obtain a reference solution we have solved the problem with a previous version of the code [61] for the special case where the spheres are comprised of an isotropic dielectric material with $\overline{\boldsymbol{\varepsilon}}_3 = 2\varepsilon_0\overline{\mathbf{I}}$ and $\overline{\boldsymbol{\mu}}_3 = \mu_0\overline{\mathbf{I}}$. For the calculation of $[S_{11}]$ in this case we have performed the MoM solution of the Poggio-Miller-Chang-Harrington-Wu-Tai SIE [14], [15] on the surface of the sphere inside a brick [54] by expanding electric and magnetic surface current densities with $N_O = 2 \times 294 = 588$ surface divergence-conforming vector basis functions [72] of the same type as in (38a), (38b) or (40).

In assembling the system (53) we have obtained the algebraic LEGO operator $[L_{\rm LEGO}]$ through (59) by employing $N_C = 30$ coupled eigencurrents out of $N_{C,\max} = \min\{2N_F, N_O\} = 1800$. Likewise, we have constructed the system given by [61, Eqs. (9), (14)] by using $N_C = 30$ coupled eigencurrents out of $N_{C,\max} = \min\{2N_F, N_O\} = 588$. Therefore, in both cases the reduced inverse scattering operator $[\tilde{S}_{\rm CC}]^{-1}$ in (58) has the rank $N_C N_D = 60$. Then, from the knowledge of $[J_{\rm A}]$ and $[q^{\rm s}]$ we have computed the 2×2

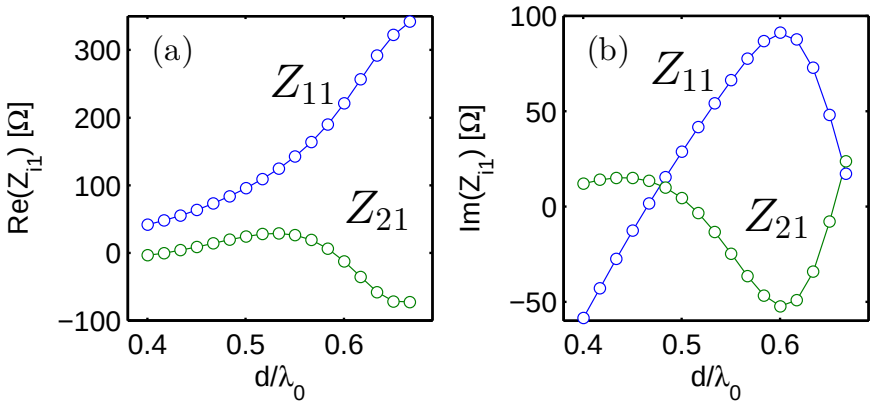

Fig. 6: Impedance matrix entries for the problem of Fig. 5: real (a) and imaginary (b) parts versus the electric length of the dipoles; (−) old LEGO-EFIE with SIE inside bricks [61], (○) LEGO-EFIE (53) and VIE inside bricks [62]. *Data*: $\varepsilon_1 = \varepsilon_2 = \varepsilon_0$, $\bar{\varepsilon}_3 = 2\varepsilon_0\bar{\mathbf{I}}$, $\mu_1 = \mu_2 = \mu_3 = \mu_0$, $N_C = 30$. (After [57].)

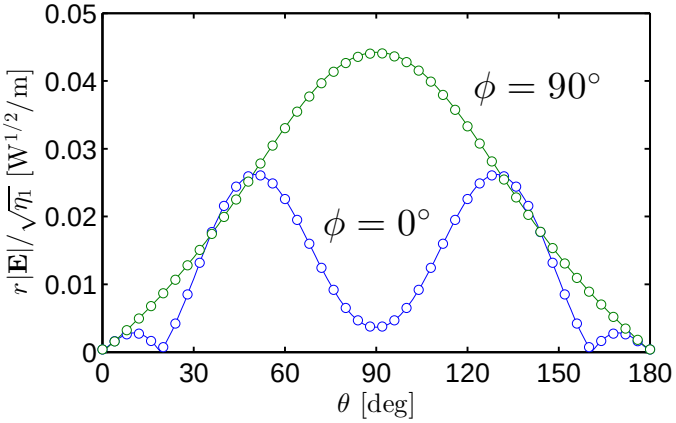

Fig. 7: Normalized radiated electric field versus the elevation angle (θ) for the problem of Fig. 5; (−) old LEGO-EFIE with SIE inside bricks [61], (○) LEGO-EFIE (53) and VIE inside bricks [62]. *Data*: see caption of Fig. 6; each port excited with $V_G = 1$ V, $d/\lambda_0 = 0.467$. (After [57].)

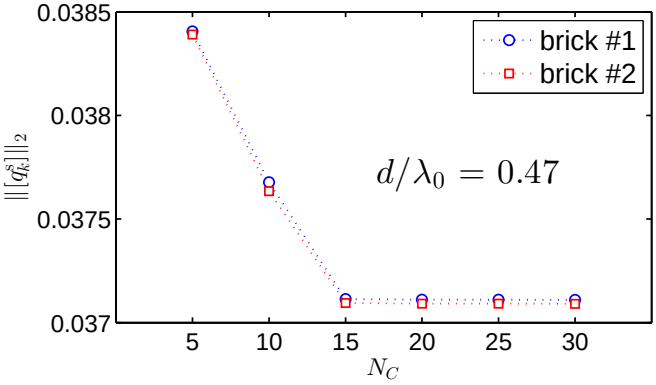

Fig. 8: Convergence of EEM: L_2-norm of $[q_k^s]$, $k = 1, 2$, versus number of coupled eigencurrents (N_C) for the antenna problem of Fig. 5. *Data*: see caption of Fig. 9. (After [57].)

antenna impedance matrix for seventeen frequency samples in the range $f \in [120, 200]$ MHz, and the normalized radiated field at $f = 140$ MHz.

The entries Z_{11} and Z_{21} of the antenna impedance matrix are plotted in Fig. 6 versus the dipole electric length d/λ_0. The magnitude of the radiated electric field is plotted in Fig. 7 as a function of the elevation angle (θ) in the half-planes $\phi = 0°$ and $\phi = 90°$ at $f = 140$ MHz. Since the results show perfect agreement, we can conclude that the LEGO-EFIE approach with VIE is not only viable, but that it has been implemented correctly.

B. Convergence of EEM with N_C

It is interesting to investigate how well the solution of (52), (53) converges when the number $N_C \leq \min\{2N_F, N_O\}$ of coupled eigencurrents is increased, because the latter have a direct impact on the accuracy of the reduced scattering operator $[\tilde{S}_{\rm CC}]$ and hence, on $[L_{\rm LEGO}]$ in (59).

Towards this end we have repeatedly solved the antenna problem of Fig. 5 at $f = 140$ MHz ($d/\lambda_0 = 0.47$) by using $N_C \in \{5, 10, 15, 20, 25, 30\}$ coupled eigencurrents. Accordingly, we have determined the impedance matrix from $[J_{\rm A}]$ and the radiated field from both $[J_{\rm A}]$ and $[q^{\rm s}]$. The L_2-norms of $[q_k^{\rm s}]$, $k = 1, 2$ are shown in Fig. 8, whereas the entries Z_{11} and Z_{21} of the impedance matrix are plotted in Fig. 9.

It is apparent that, for the problem at hand, convergence is reached when we employ just $N_C = 15$ coupled eigencurrents out of 1800. As can be expected, the convergence of the radiated fields is even more rapid. This can be ascertained from Fig. 10, in which the magnitude of the normalized electric field obtained with $N_C \in \{10, 20\}$ at $f = 140$ MHz is compared to the same quantity computed with $N_C = 30$, the latter being assumed as a reference solution in view of Fig. 8.

In Section V we have argued that the coupled (uncoupled) eigencurrents of the algebraic scattering operator are associated with the larger (smaller) eigenvalues $\lambda_q^{(k)}$ of $[S_{kk}]$. To support this speculation, in Fig. 11 we have plotted the spectrum of $[S_{11}]$ pertinent to the antenna-objects problem of Fig. 5 again at $f = 140$ MHz. As can be seen, the eigenvalues decay very fast (exponentially) until they drop down to the threshold of numerical noise for double-precision floating-point calculations.

In general, this trend is common to all EM bricks containing a PEC [66] or a penetrable object [62], [66]. However,

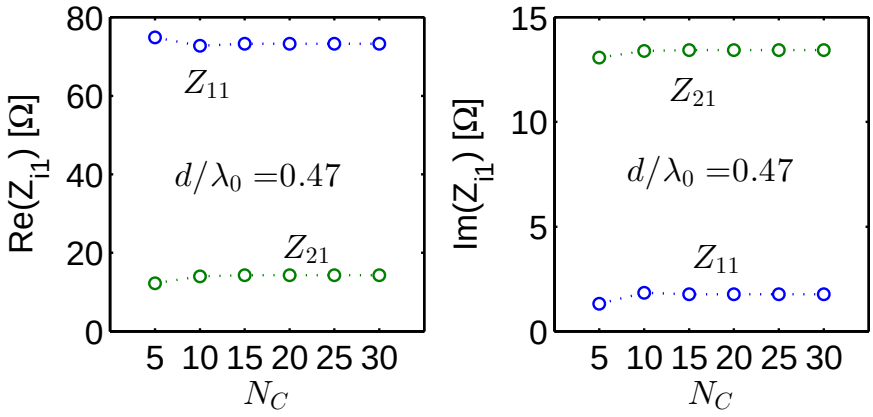

Fig. 9: Convergence of EEM: impedance-matrix entries (Z_{i1}) versus number of coupled eigencurrents (N_C) for the antenna problem of Fig. 5; the markers ($\circ$) are joined with a dotted line for visualization's sake. *Data*: $\varepsilon_1 = \varepsilon_2 = \varepsilon_0$, $\overline{\overline{\varepsilon}}_3 = (4\hat{\mathbf{x}}\hat{\mathbf{x}} + 2\hat{\mathbf{y}}\hat{\mathbf{y}} + 2\hat{\mathbf{z}}\hat{\mathbf{z}})\varepsilon_0$, $\mu_1 = \mu_2 = \mu_3 = \mu_0$. (After [57].)

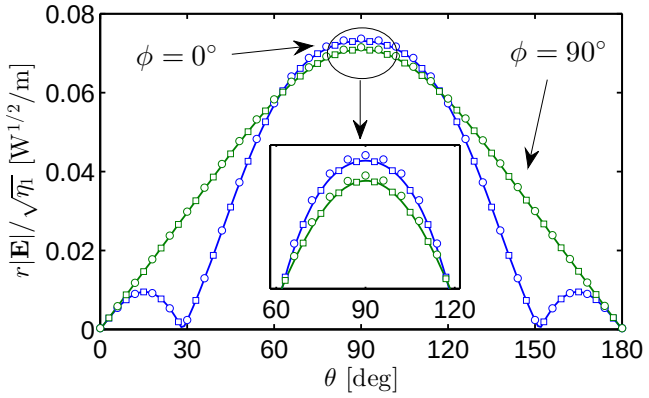

Fig. 10: Convergence of EEM: normalized radiated electric field versus elevation angle (θ) for different numbers of coupled eigencurrents (N_C) for the problem of Fig. 5; ($\circ$) $N_C = 10$, ($\square$) $N_C = 20$, ($-$) $N_C = 30$. Inset: close-up of the electric field. *Data*: see caption of Fig. 9; each port excited with $V_G = 1$ V, $d/\lambda_0 = 0.467$. (After [57].)

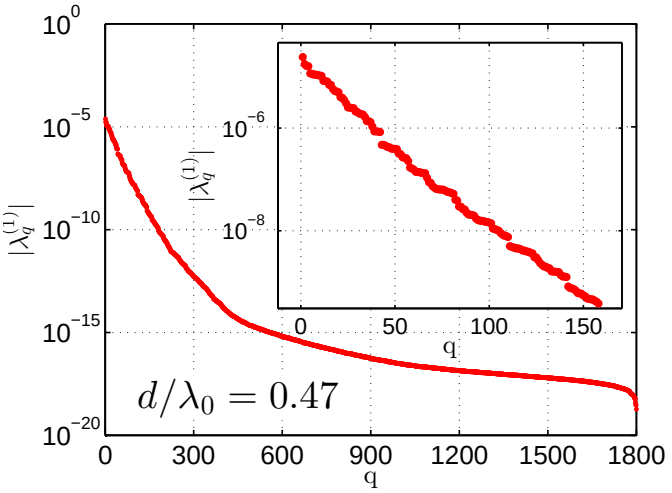

Fig. 11: Convergence of EEM: spectrum of eigenvalues of $[S_{11}]$ as a function of their index $q = 1, \ldots, 2N_F$ for the antenna-objects system of Fig. 5 at $f = 140$ MHz. Inset: close-up of the eigenvalues pertinent to the strongly coupled eigencurrents.

$|\lambda_1^{(k)}|$ depends substantially on the relative size of brick and embedded object and the constitutive parameters thereof. Besides, a sharp threshold separating the coupled eigencurrents from the uncoupled ones may appear (cf. [66, Figs. 2-4]), if $2N_O < 2N_F$ or $N_O < 2N_F$, that is, the number of basis functions employed to solve (31) is smaller than the number of expansion functions introduced over $\partial\mathcal{D}_k$. Actually, in this instance the algebraic scattering operator (44) is obviously rank-deficient.

VII. Application Example: Plasma Antenna Array

A Gaseous Plasma Antenna (GPA) is a plasma discharge (usually, in the form of a dielectric tube filled with gas) in which the generated plasma behaves as a conducting medium when the tube is energized, and this enables the tube to transmit and receive EM waves [6], [74]. GPAs have many potential advantages over conventional metallic antennas [75], namely:

- They are reconfigurable with respect to radiation pattern, frequency, bandwidth [5], [6].
- They can be reconfigured electrically — rather than mechanically — on time scales that are on the order of microseconds to milliseconds.
- They have lower thermal noise and minimise signal degradation, as they are activated only while communication takes place.
- They are virtually "transparent" above the plasma frequency, and become "invisible" once turned off.

Also, GPAs operating at different frequencies do not interfere with one another, a property which makes it possible to stack arrays of plasma antennas.

A Plasma Antenna Array (PAA) is a cluster of GPAs and possibly conventional metallic elements [74]. In addition to having all the advantages of baseline GPAs, PAAs allow (i) steering the beam and (ii) improving directivity by adding nulls to the radiation pattern. Moreover, an array of plasma discharges surrounding a radiating element — which can be either metallic or a GPA — effectively realizes a "plasma

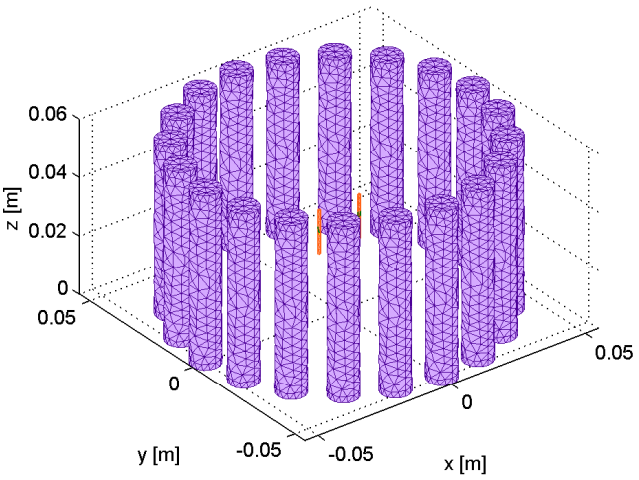

(a)

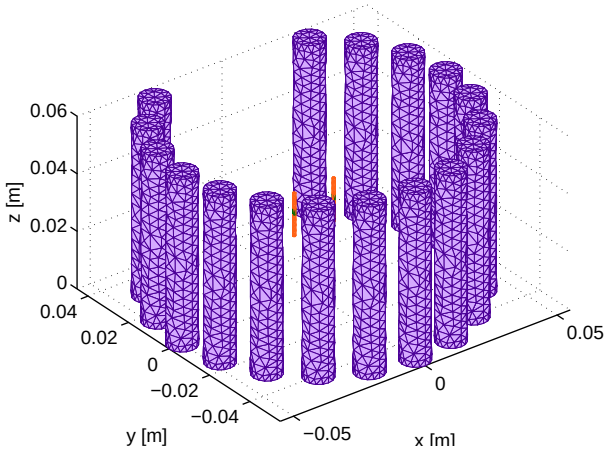

(b)

Fig. 12: Modelling a reconfigurable PAA with LEGO: (a) two PEC center-fed cylindrical dipoles surrounded by a circular screen of $N_D = 20$ plasma tubes; (b) same as before, but with three plasma tubes switched off ($N_D = 17$). *Data*: radius of the plasma screen 5 cm. (Also see caption of Figs. 13, 14).

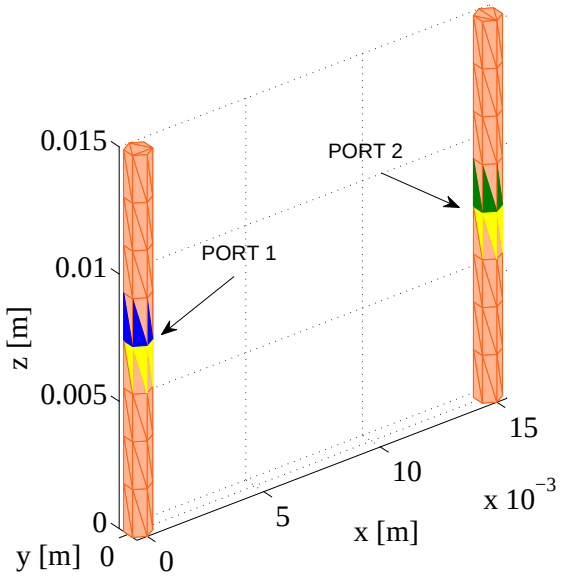

Fig. 13: Modelling a reconfigurable PAA with LEGO: 3-D triangular tessellation of two PEC center-fed cylindrical dipoles. *Data*: height of dipoles (d) 15 mm, diameter of dipoles 1 mm, separation of dipoles along the x-axis 15 mm, $N_A = 312$.

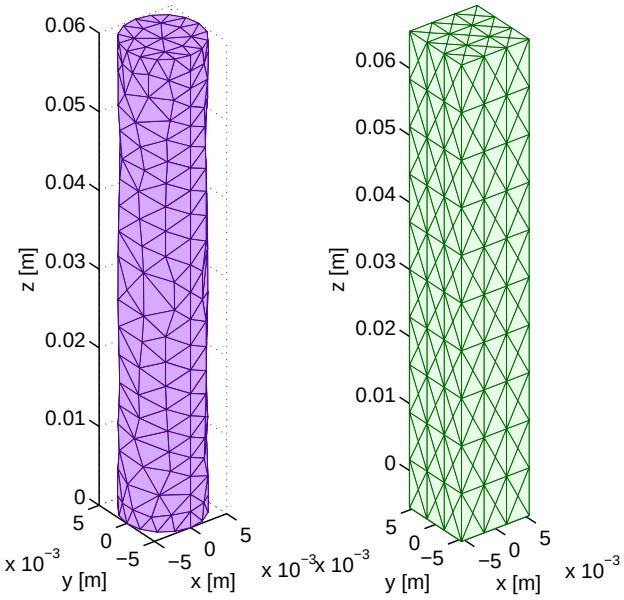

Fig. 14: Modelling a reconfigurable PAA with LEGO: (a) tetrahedral mesh of a plasma tube; (b) surface mesh of the brick that embeds the tube. *Data*: diameter of tube 10 mm, height of tube 60 mm, width of brick 11 mm, height of brick 71 mm, $N_O = 3056$, $2N_F = 1656$.

blanket" of sorts that can be used to shield unwanted incoming EM waves and open "windows" in selected positions so as to let outward EM waves through.

As a practical realization of these concepts, we consider the PAA shown in Fig. 12. The radiating element is a linear array of two PEC center-fed cylindrical dipoles (Fig. 13), whereas the plasma blanket is comprised of $N_D = 20$ cylindrical plasma tubes arranged in a circular fashion around the dipoles (Fig. 12a). This PAA is reconfigurable primarily in the sense that the plasma tubes can selectively be switched on and off as needed to create windows for beam-forming and beam-steering. For instance, the PAA operating with only $N_D = 17$ tubes switched on is shown in Fig. 12b.

In order to apply the hybrid LEGO-EFIE method, we embed each plasma tube in a cuboidal EM brick, as shown in Fig. 14. The width and height of the bricks are 11 mm and 71 mm, respectively. The background and host media are free space; therefore $\varepsilon_1 = \varepsilon_2 = \varepsilon_0$. However, since the plasma (medium ③) is modelled with a dyadic permittivity, then $\overline{\boldsymbol{\mu}}_3 = \mu_0 \overline{\mathbf{I}}$, and (31) takes on the special form given by (74), (75a), (75b) in Appendix B. The cylindrical plasma tubes are evenly distributed on a circle with radius of 50 mm; each tube is aligned with the z-axis, and has a diameter of 10 mm and a height of 60 mm. The plasma is assumed cold, weakly ionized, collisional, and magnetized. Then, in a system of Cartesian coordinates with magneto-static field $\mathbf{B}_0 = B_0 \hat{\mathbf{z}}$, the dyadic

permittivity $\overline{\overline{\varepsilon}}_3$ reads

$$\overline{\overline{\varepsilon}}_3 = \varepsilon_0 \begin{bmatrix} S & \mathrm{j}D & 0 \\ -\mathrm{j}D & S & 0 \\ 0 & 0 & P \end{bmatrix}, \tag{63}$$

where

$$S \equiv 1 - \sum_{\xi} \frac{\omega_{p\xi}^2(\omega - \mathrm{j}\nu_\xi)}{\omega[(\omega - \mathrm{j}\nu_\xi)^2 - \omega_{c\xi}^2]}, \tag{64a}$$

$$D \equiv \sum_{\xi} \frac{\sigma_\xi \omega_{c\xi}}{\omega} \frac{\omega_{p\xi}^2}{(\omega - \mathrm{j}\nu_\xi)^2 - \omega_{c\xi}^2}, \tag{64b}$$

$$P \equiv 1 - \sum_{\xi} \frac{\omega_{p\xi}^2}{\omega(\omega - \mathrm{j}\nu_\xi)}, \tag{64c}$$

are the Stix parameters [76], with $\omega_{p\xi} \equiv [n_\xi q_\xi^2/(\varepsilon_0 m_\xi)]^{1/2}$ the plasma frequency, $\omega_{c\xi} \equiv \sigma_\xi q_\xi B_0/m_\xi$ the gyrofrequency, ν_ξ the collision frequency, and $\sigma_\xi = \pm$ the particle charge sign; the subscript 'ξ' refers to the plasma species. By letting $\overline{\overline{\varepsilon}}_3$ be a function of position, profiles of plasma density, magnetic field, electron temperature, and neutral pressure can be handled; however, in the numerical experiments described below $\overline{\overline{\varepsilon}}_3$ is considered constant.

The PEC dipoles both have a diameter of 1 mm and a height of 15 mm, they are aligned with the z-axis, and are placed at a distance of 15 mm along the x-axis (see Fig. 13). They are excited in phase with $V_G = 1$ V [cf. (14)] at the frequency $f = 10$ GHz.

The surface (volume) basis functions on the boundary of a brick (in a plasma tube) are $2N_F = 1656$ ($N_O = 3056$). The current density induced over the dipoles is represented by means of $N_A = 312$ surface basis functions. The problem in Fig. 12a is modelled with $N_D = 20$ EM bricks, whereas only $N_D = 17$ bricks are employed for the PAA with a window in Fig. 12b.

We have investigated the role played by plasma discharge parameters in the two configurations of Fig. 12. Specifically, the plasma is made of argon ions (Ar^+) and electrons with the same uniform density $n_0 = 10^{19}$ m^{-3}. The chosen neutral pressure and electron temperature are such that the electron collision frequency is $\nu_e = 89$ GHz, and the collision frequency of the argon ions is negligible with respect to ν_e. Two scenarios in terms of magneto-static field have been considered: (i) $B_0 = 0$ T (non-magnetized case); and (ii) $B_0 = 0.1$ T (magnetized case). With these positions, the Stix parameters take on the values listed in Table I.

TABLE I: Plasma parameters for the PAAs of Fig. 12

	$B_0 = 0$ [T]
S	$-7.061727403150083 - \mathrm{j}0.013250915072170$
D	0
P	$-7.061727403150083 - \mathrm{j}0.013250915072170$
	$B_0 = 0.1$ [T]
S	$-7.747114953842780 - \mathrm{j}0.016822229467298$
D	$0.008733555419741 - \mathrm{j}2.448490150087137$
P	$-7.061727403150083 - \mathrm{j}0.013250915072170$

The antenna gain function $g(\theta, \phi)$ relative to the ideal isotropic radiator [68] is plotted in Figs. 15 and 16 for the two scenarios. For the sake of reference, the gain of the two-dipole array in the case when all the plasma tubes are switched off (solid blue line) is superimposed to each plot to help appreciate the combined effect of the plasma blanket (window) and the plasma discharge parameters.

In particular, from Fig. 15a we notice that the PAA with $N_D = 20$ energized plasma tubes exhibits six narrow main lobes in the E-plane for $\phi \in \{90°, 270°\}$; correspondingly, the maximum gain is lower that that of the two-dipole array in free space. As expected, the plasma window renders the gain asymmetric, and enhances the three main lobes in the $\phi = 90°$ half-plane. In the H-plane (Fig. 15b), the angular distribution of power of the PAA with $N_D = 20$ energized plasma tubes is similar to that of the two-dipole array in free space, but the gain is significantly smaller. When a window is opened in the blanket, the beam-forming effect of the active plasma tubes becomes evident: A narrow main lobe appears in the broadside direction $\theta = \phi = 90°$, while the backward radiation is reduced.

Quite similar observations apply to the gain in the second scenario (i.e., magnetized plasma tubes) reported in Figs. 16a and 16b. In fact, a non-null magneto-static field makes the plasma non-reciprocal [cf. (63)], which in turn results in asymmetric gain for $\phi \in \{90°, 270°\}$ in the E-plane for the case $N_D = 20$ plasma tubes. Furthermore, in the H-plane the magneto-static field reduces the maximum gain in the case of the windowed PAA as compared to the corresponding configuration with $B_0 = 0$ T (Fig. 15b).

We conclude this discussion with a comment on the efficiency. While it is clear from Figs. 15 and 16 that the PAA under investigation is capable of beam-forming and beam-steering, we also note that the maximum gain is lower than that of the two-dipole array alone in the H-plane and for some directions in the E-plane, owing to the lossy nature of the plasma. Therefore, at least in our example higher input power should be provided to exploit the reconfigurability afforded by PAAs while preserving the level of the maximum gain.

As regards the computational performance of the hybrid LEGO-EFIE approach, the size of the algebraic total inverse scattering operator $[S]^{-1}$ in (48) is $2N_F N_D = 33120$ for the PAA with $N_D = 20$ tubes and $2N_F N_D = 28152$ for the PAA with a window ($N_D = 17$). However, by applying the EEM with $N_C = 50$ coupled eigencurrents out of $N_{C,\max} = \min\{2N_F, N_O\} = 1656$, the calculation of $[L_{\mathrm{LEGO}}]$ in (53) boils down to inverting a matrix $[\tilde{S}_{\mathrm{CC}}]^{-1}$ with a rank $N_C N_D \in \{1000, 850\}$. More importantly, the size of the system matrix in (53) is just $N_A = 312$, i.e., determined by the number of basis functions used to expand $\mathbf{J}_A$ on the dipoles. Furthermore, as all the plasma tubes have the same shape and EM properties, only one algebraic scattering operator, say $[S_{11}]$, must be computed; therefore, the solution of the VIE (31), which is time-consuming, has to be carried out only once for each of the scenarios described above. In contrast, the direct solution of the problems of Fig. 12 with a

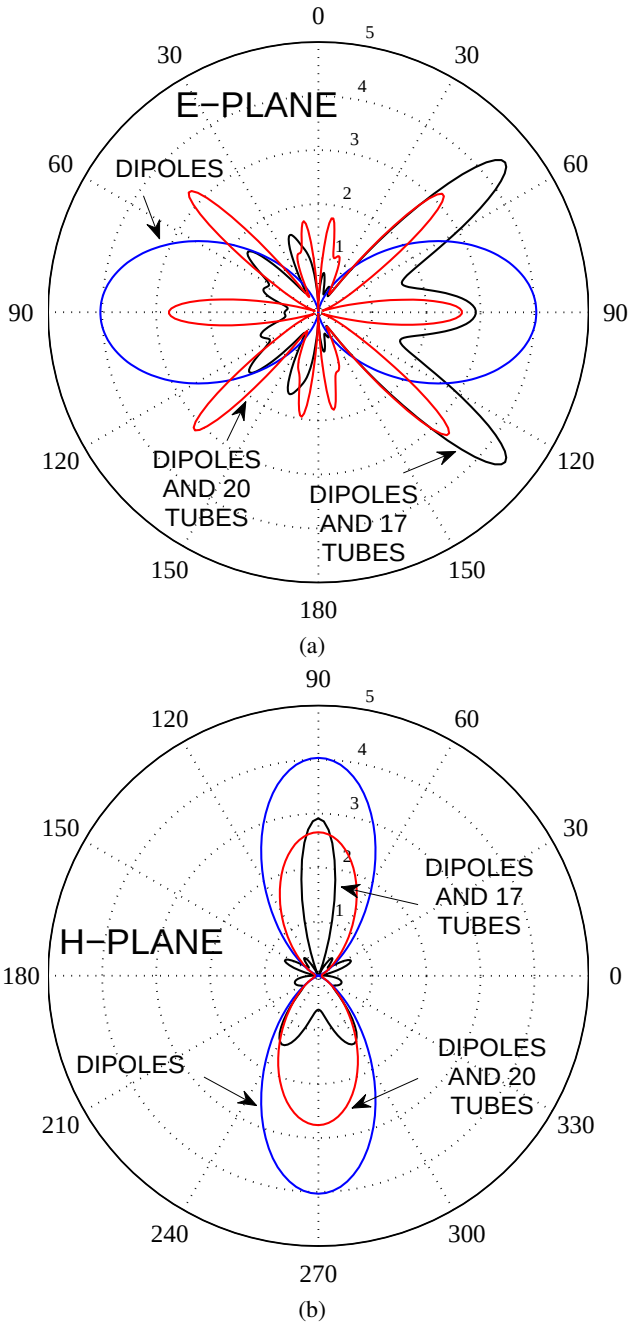

Fig. 15: Modelling a reconfigurable PAA with LEGO: antenna gain (natural units) for various configurations; (a) E-plane ($\phi \in \{90°, 270°\}$), (b) H-plane ($\theta = 90°$). *Data*: each antenna port excited with $V_G = 1$ V at $f = 10$ GHz, plasma density $n_0 = 10^{19}$ m^{-3}, plasma magnetizing field $\mathbf{B}_0 = 0$ T.

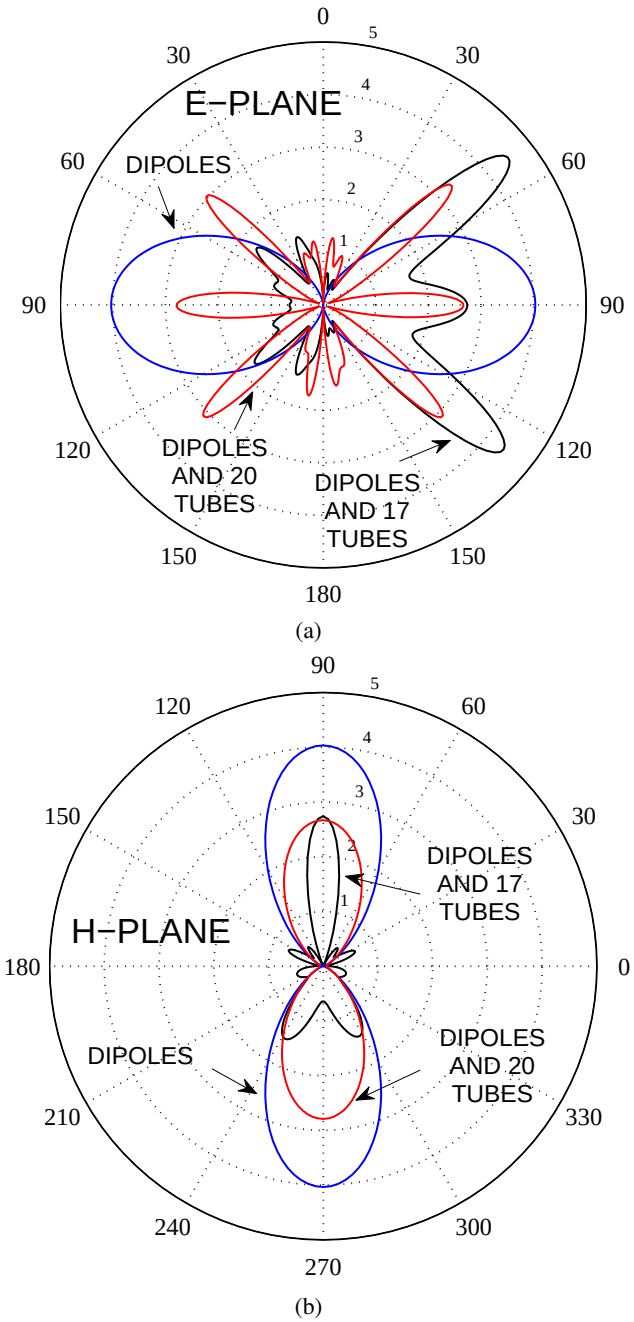

Fig. 16: Modelling a reconfigurable PAA with LEGO: antenna gain (natural units) for various configurations; (a) E-plane ($\phi \in \{90°, 270°\}$), (b) H-plane ($\theta = 90°$). *Data*: each antenna port excited with $V_G = 1$ V at $f = 10$ GHz, plasma density $n_0 = 10^{19}$ m^{-3}, plasma magnetizing field $\mathbf{B}_0 = 0.1$ T.

VSIE formulation (e.g., [7]) would require the solution of a system with rank $N_O N_D + N_A \in \{61432, 52264\}$.

VIII. Conclusion

The hybrid LEGO-EFIE method uses EM bricks in tandem with the standard EFIE to model complex problems, which involve conventional PEC antennas or scatterers and media with anisotropic constitutive parameters. The strategy is particularly well-suited when the problem at hand comes naturally decomposed in many separated parts. The calculation of the scattering operators of the bricks with the baseline MoM entails the inversion of one small VIE at a time, which is extremely competitive over the solution of coupled VSIEs for the entire problem. Besides, the very introduction of scattering operators enables us to reduce the degrees of freedom, because expanding the unknown equivalent current densities on the boundary of a brick usually requires fewer basis functions than are necessary to solve the VIE for the embedded anisotropic

object. As the modularity of the approach enables us to combine and recycle the EM bricks with few restrictions, the time required to analyze similar structures (such as the PAAs addressed in Section VII) can also be considerably reduced. Finally, the usage of the eigencurrents of the scattering operators as locally entire-domain basis functions over the boundaries of the bricks enables us to handle and compress the weak form of the LEGO functional equations to derive the modified EFIE efficiently.

APPENDIX A
PROPAGATORS USED IN LEGO

Listed in this appendix are the propagators involved in the definition of S_{kk}, T_{kn}, $(\mathsf{T}_{\mathrm{OA}})_k$, and $(\mathsf{P}_{\mathrm{AO}})_k$.

In what follows, k_1 denotes the wavenumber in medium ①, $\mathbf{r}$ ($\mathbf{r}'$) denotes the field (source) point, $\bar{\mathbf{I}}_{\mathrm{s}}$ is the transverse unit dyadic tangential to $\partial\mathcal{D}_{k,n}$ or $\mathcal{S}_{\mathrm{A}}$. The surface 'del' operator is defined as $\nabla_{\mathrm{s}} = \bar{\mathbf{I}}_{\mathrm{s}} \cdot \nabla$, and $\nabla'_{\mathrm{s}} = -\nabla_{\mathrm{s}}$ means differentiation with respect to $\mathbf{r}'$. The specification 'PV' before an integral sign means that integration is performed in the Cauchy principle value sense, while d^2r', d^3r' represent the area and the volume elements, respectively. The unit normal $\hat{\mathbf{n}}_k$ to $\partial\mathcal{D}_k$ points inward $\mathcal{D}_k$ (Fig. 1b).

A. Brick-to-brick interaction

The propagators $\mathsf{P}^{\mathrm{i}}_{kk}$, $\mathsf{P}^{\mathrm{s}}_{kk}$, P_{kn} are 2×2 abstract matrices whose entries are dyadic integro-differential operators involving the Green's function $G_1(R)$ in (17).

$$\mathsf{P}^{\mathrm{i}}_{kk} : \partial\mathcal{D}_k \to \partial\mathcal{D}_k$$
(from incident currents to incident fields)

$$(\mathsf{P}^{\mathrm{i}}_{kk})_{11}\{\circ\} \equiv -\mathrm{j}k_1 \int_{\partial\mathcal{D}_k} \mathrm{d}^2r' G_1(R)\, \bar{\mathbf{I}}_{\mathrm{s}} \cdot \{\circ\} - \frac{\mathrm{j}\nabla_{\mathrm{s}}}{k_1} \int_{\partial\mathcal{D}_k} \mathrm{d}^2r' G_1(R) \nabla'_{\mathrm{s}} \cdot \{\circ\}, \quad \mathbf{r} \in \partial\mathcal{D}_k, \tag{65a}$$

$$(\mathsf{P}^{\mathrm{i}}_{kk})_{12}\{\circ\} \equiv -\mathrm{PV} \int_{\partial\mathcal{D}_k} \mathrm{d}^2r' \nabla'_{\mathrm{s}} G_1(R) \times \bar{\mathbf{I}}_{\mathrm{s}} \cdot \{\circ\} + \frac{1}{2}\hat{\mathbf{n}}_k \times \bar{\mathbf{I}}_{\mathrm{s}} \cdot \{\circ\}, \quad \mathbf{r} \in \partial\mathcal{D}_k, \tag{65b}$$

$$(\mathsf{P}^{\mathrm{i}}_{kk})_{21}\{\circ\} \equiv \mathrm{PV} \int_{\partial\mathcal{D}_k} \mathrm{d}^2r' \nabla_{\mathrm{s}} G_1(R) \times \bar{\mathbf{I}}_{\mathrm{s}} \cdot \{\circ\} - \frac{1}{2}\hat{\mathbf{n}}_k \times \bar{\mathbf{I}}_{\mathrm{s}} \cdot \{\circ\}, \quad \mathbf{r} \in \partial\mathcal{D}_k, \tag{65c}$$

$$(\mathsf{P}^{\mathrm{i}}_{kk})_{22}\{\circ\} = -(\mathsf{P}^{\mathrm{i}}_{kk})_{11}\{\circ\}, \tag{65d}$$

$$\mathsf{P}^{\mathrm{s}}_{kk} : \partial\mathcal{D}_k \to \partial\mathcal{D}_k$$
(from scattered currents to scattered fields)

$$(\mathsf{P}^{\mathrm{s}}_{kk})_{11}\{\circ\} \equiv -\mathrm{j}k_1 \int_{\partial\mathcal{D}_k} \mathrm{d}^2r' G_1(R)\, \bar{\mathbf{I}}_{\mathrm{s}} \cdot \{\circ\} - \frac{\mathrm{j}\nabla_{\mathrm{s}}}{k_1} \int_{\partial\mathcal{D}_k} \mathrm{d}^2r' G_1(R) \nabla'_{\mathrm{s}} \cdot \{\circ\}, \quad \mathbf{r} \in \partial\mathcal{D}_k, \tag{66a}$$

$$(\mathsf{P}^{\mathrm{s}}_{kk})_{12}\{\circ\} \equiv -\mathrm{PV} \int_{\partial\mathcal{D}_k} \mathrm{d}^2r' \nabla'_{\mathrm{s}} G_1(R) \times \bar{\mathbf{I}}_{\mathrm{s}} \cdot \{\circ\} - \frac{1}{2}\hat{\mathbf{n}}_k \times \bar{\mathbf{I}}_{\mathrm{s}} \cdot \{\circ\}, \quad \mathbf{r} \in \partial\mathcal{D}_k, \tag{66b}$$

$$(\mathsf{P}^{\mathrm{s}}_{kk})_{21}\{\circ\} \equiv \mathrm{PV} \int_{\partial\mathcal{D}_k} \mathrm{d}^2r' \nabla_{\mathrm{s}} G_1(R) \times \bar{\mathbf{I}}_{\mathrm{s}} \cdot \{\circ\} + \frac{1}{2}\hat{\mathbf{n}}_k \times \bar{\mathbf{I}}_{\mathrm{s}} \cdot \{\circ\}, \quad \mathbf{r} \in \partial\mathcal{D}_k, \tag{66c}$$

$$(\mathsf{P}^{\mathrm{s}}_{kk})_{22}\{\circ\} = -(\mathsf{P}^{\mathrm{s}}_{kk})_{11}\{\circ\}, \tag{66d}$$

$$\mathsf{P}_{nk} : \partial\mathcal{D}_n \to \partial\mathcal{D}_k,\ n \neq k$$
(from scattered currents to incident fields)

$$(\mathsf{P}_{kn})_{11}\{\circ\} = (\mathsf{P}_{kn})_{12}\{\circ\} \equiv \bar{\mathbf{0}} \cdot \{\circ\}, \tag{67a}$$

$$(\mathsf{P}_{kn})_{21}\{\circ\} \equiv \mathrm{PV} \int_{\partial\mathcal{D}_n} \mathrm{d}^2r' \nabla_{\mathrm{s}} G_1(R) \times \bar{\mathbf{I}}_{\mathrm{s}} \cdot \{\circ\} + \frac{1}{2}\hat{\mathbf{n}}_n \times \bar{\mathbf{I}}_{\mathrm{s}} \cdot \{\circ\}, \quad \mathbf{r} \in \partial\mathcal{D}_k, \tag{67b}$$

$$(\mathsf{P}_{kn})_{22}\{\circ\} \equiv \mathrm{j}k_1 \int_{\partial\mathcal{D}_n} \mathrm{d}^2r' G_1(R)\, \bar{\mathbf{I}}_{\mathrm{s}} \cdot \{\circ\} + \frac{\mathrm{j}\nabla_{\mathrm{s}}}{k_1} \int_{\partial\mathcal{D}_n} \mathrm{d}^2r' G_1(R) \nabla'_{\mathrm{s}} \cdot \{\circ\}, \quad \mathbf{r} \in \partial\mathcal{D}_k, \tag{67c}$$

The entries $(\mathsf{P}_{kn})_{11}$ and $(\mathsf{P}_{kn})_{12}$ are null, because the propagator $\mathsf{P}^{\mathrm{i}}_{kk}$ [cf. (36a)] requires only the magnetic field to determine the equivalent incident currents.

B. Brick-to-object and object-to-brick interaction

In the special case when the anisotropic body is either dielectric (with $\overline{\boldsymbol{\mu}}_3 = \mu_1\bar{\mathbf{I}}$) or magnetic (with $\overline{\boldsymbol{\varepsilon}}_3 = \varepsilon_1\bar{\mathbf{I}}$), the propagators P_{ok} ($\mathsf{P}_{k\,\mathrm{o}}$) reduce to 1×2 (2×1) abstract matrices whose entries are dyadic integro-differential operators involving the Green's function $G_1(R)$ in (17). The contrast dyadics $\overline{\boldsymbol{\alpha}}_e(\mathbf{r})$ and $\overline{\boldsymbol{\alpha}}_h(\mathbf{r})$ are defined in (30a) and (30b).

Anisotropic dielectric body

$$\mathsf{P}_{ok} : \partial\mathcal{D}_k \to \mathcal{V}_{\mathrm{O}}$$
(from incident currents to incident electric flux density)

$$(\mathsf{P}_{ok})_{11}\{\circ\} \equiv -\mathrm{j}k_1 \int_{\partial\mathcal{D}_k} \mathrm{d}^2r' G_1(R)\, \bar{\mathbf{I}}_{\mathrm{s}} \cdot \{\circ\} - \frac{\mathrm{j}\nabla_{\mathrm{s}}}{k_1} \int_{\partial\mathcal{D}_k} \mathrm{d}^2r' G_1(R) \nabla'_{\mathrm{s}} \cdot \{\circ\}, \quad \mathbf{r} \in \mathcal{V}_{\mathrm{O}}, \tag{68a}$$

$$(\mathsf{P}_{ok})_{12}\{\circ\} \equiv -\mathrm{PV} \int_{\partial\mathcal{D}_k} \mathrm{d}^2r' \nabla'_{\mathrm{s}} G_1(R) \times \bar{\mathbf{I}}_{\mathrm{s}} \cdot \{\circ\} - \frac{1}{2}\hat{\mathbf{n}}_k \times \bar{\mathbf{I}}_{\mathrm{s}} \cdot \{\circ\}, \quad \mathbf{r} \in \mathcal{V}_{\mathrm{O}}, \tag{68b}$$

Anisotropic magnetic body

$$\mathsf{P}_{ok} : \partial\mathcal{D}_k \to \mathcal{V}_{\mathrm{O}}$$

(from incident currents to incident magnetic flux density)

$$(\mathsf{P}_{\mathrm{o}k})_{21} \equiv -\mathrm{PV}\int_{\partial\mathcal{D}_k} \mathrm{d}^2 r' \nabla'_{\mathrm{s}} G_1(R) \times \bar{\mathbf{I}}_{\mathrm{s}} \cdot \{\circ\} - \frac{1}{2}\hat{\mathbf{n}}_k \times \bar{\mathbf{I}}_{\mathrm{s}} \cdot \{\circ\}, \quad \mathbf{r} \in \mathcal{V}_{\mathrm{O}}, \quad (69a)$$

$$(\mathsf{P}_{\mathrm{o}k})_{22}\{\circ\} \equiv \mathrm{j}k_1 \int_{\partial\mathcal{D}_k} \mathrm{d}^2 r' G_1(R)\, \bar{\mathbf{I}}_{\mathrm{s}} \cdot \{\circ\} + \frac{\mathrm{j}\nabla_{\mathrm{s}}}{k_1} \int_{\partial\mathcal{D}_k} \mathrm{d}^2 r' G_1(R) \nabla'_{\mathrm{s}} \cdot \{\circ\}, \quad \mathbf{r} \in \mathcal{V}_{\mathrm{O}}, \quad (69b)$$

Anisotropic dielectric body

$\mathsf{P}_{k\,\mathrm{o}} : \mathcal{V}_{\mathrm{O}} \to \partial\mathcal{D}_k$

(from total electric flux density to scattered fields)

$$(\mathsf{P}_{k\,\mathrm{o}})_{11}\{\circ\} \equiv \overline{\mathbf{0}} \cdot \{\circ\}, \quad (70a)$$

$$(\mathsf{P}_{k\,\mathrm{o}})_{21}\{\circ\} \equiv \mathrm{j}k_1 \int_{\mathcal{V}_{\mathrm{O}}} \mathrm{d}^3 r'\, \bar{\mathbf{I}}_{\mathrm{s}} \cdot \nabla G_1(R) \times \overline{\boldsymbol{\alpha}}_e(\mathbf{r}') \cdot \{\circ\}, \quad \mathbf{r} \in \partial\mathcal{D}_k, \quad (70b)$$

Anisotropic magnetic body

$\mathsf{P}_{k\,\mathrm{o}} : \mathcal{V}_{\mathrm{O}} \to \partial\mathcal{D}_k$

(from total magnetic flux density to scattered fields)

$$(\mathsf{P}_{k\,\mathrm{o}})_{12}\{\circ\} \equiv \overline{\mathbf{0}} \cdot \{\circ\}, \quad (71a)$$

$$(\mathsf{P}_{k\,\mathrm{o}})_{22}\{\circ\} \equiv k_1^2 \int_{\mathcal{V}_{\mathrm{O}}} \mathrm{d}^3 r' G_1(R)\, \bar{\mathbf{I}}_{\mathrm{s}} \cdot \overline{\boldsymbol{\alpha}}_h(\mathbf{r}') \cdot \{\circ\} + \nabla_{\mathrm{s}} \int_{\mathcal{V}_{\mathrm{O}}} \mathrm{d}^3 r' G_1(R) \nabla' \cdot [\,\overline{\boldsymbol{\alpha}}_h(\mathbf{r}') \cdot \{\circ\}], \quad \mathbf{r} \in \partial\mathcal{D}_k \quad (71b)$$

The entries $(\mathsf{P}_{k\,\mathrm{o}})_{11}$ and $(\mathsf{P}_{k\,\mathrm{o}})_{12}$ are null, since the propagator $\mathsf{P}^{\mathrm{s}}_{kk}$ [cf. (34)] requires only the magnetic field to determine the equivalent scattered currents.

C. Antenna-to-brick and brick-to-antenna interaction

The propagators $\mathsf{P}_{k\mathrm{A}}$ ($\mathsf{P}_{\mathrm{A}k}$) are 2×1 (1×2) abstract matrices, whose entries are dyadic integro-differential operators involving the Green's function $G_1(R)$ in (17).

$\mathsf{P}_{k\mathrm{A}} : \mathcal{S}_{\mathrm{A}} \to \partial\mathcal{D}_k$

(from antenna current to incident fields)

$$(\mathsf{P}_{k\mathrm{A}})_{11}\{\circ\} \equiv \overline{\mathbf{0}} \cdot \{\circ\}, \quad (72a)$$

$$(\mathsf{P}_{k\mathrm{A}})_{21}\{\circ\} \equiv \int_{\mathcal{S}_{\mathrm{A}}} \mathrm{d}^2 r' \nabla_{\mathrm{s}} G_1(R) \times \bar{\mathbf{I}}_{\mathrm{s}} \cdot \{\circ\}, \quad \mathbf{r} \in \partial\mathcal{D}_k, \quad (72b)$$

$\mathsf{P}_{\mathrm{A}k} : \partial\mathcal{D}_k \to \mathcal{S}_{\mathrm{A}}$

(from scattered currents to incident fields)

$$(\mathsf{P}_{\mathrm{A}k})_{11}\{\circ\} \equiv -\mathrm{j}k_1 \int_{\partial\mathcal{D}_k} \mathrm{d}^2 r' G_1(R)\, \bar{\mathbf{I}}_{\mathrm{s}} \cdot \{\circ\} - \frac{\mathrm{j}\nabla_{\mathrm{s}}}{k_1} \int_{\partial\mathcal{D}_k} \mathrm{d}^2 G_1(R) \nabla'_{\mathrm{s}} \cdot \{\circ\}, \quad \mathbf{r} \in \mathcal{S}_{\mathrm{A}}, \quad (73a)$$

$$(\mathsf{P}_{\mathrm{A}k})_{12}\{\circ\} \equiv \int_{\partial\mathcal{D}_k} \mathrm{d}^2 r' \nabla_{\mathrm{s}} G_1(R) \times \bar{\mathbf{I}}_{\mathrm{s}} \cdot \{\circ\}, \quad \mathbf{r} \in \mathcal{S}_{\mathrm{A}}, \quad (73b)$$

The entry $(\mathsf{P}_{k\mathrm{A}})_{11}$ is null, because the propagator $\mathsf{P}^{\mathrm{i}}_{kk}$ in (36a) requires only the magnetic field to determine the equivalent incident currents. Provided the antenna and the conducting parts do not touch the bricks, it is not necessary to take the principal value of the integrals (72b) and (73b) nor do they contribute a residue, for the kernel is never singular.

APPENDIX B
EXPLICIT FORMS OF (31)

In the special instance of either dielectric (with $\overline{\boldsymbol{\mu}}_3 = \mu_1 \bar{\mathbf{I}}$) or magnetic (with $\overline{\boldsymbol{\varepsilon}}_3 = \varepsilon_1 \bar{\mathbf{I}}$) anisotropic object, X_{oo} in (31) reduces to a volume integro-differential operator involving the Green's function $G_1(R)$ in (17) and either $\overline{\boldsymbol{\alpha}}_e(\mathbf{r})$ or $\overline{\boldsymbol{\alpha}}_h(\mathbf{r})$. Also, q_{o} and $F^{\mathrm{i}}_{\mathrm{o}}$ become one-element abstract column vectors.

Anisotropic dielectric body

$\mathsf{X}_{\mathrm{oo}} : \mathcal{V}_{\mathrm{O}} \to \mathcal{V}_{\mathrm{O}}$

(from flux density to flux density)

$$\mathsf{X}_{\mathrm{oo}}\{\circ\} \equiv \left[\frac{\overline{\boldsymbol{\varepsilon}}_3(\mathbf{r})}{\varepsilon_1}\right]^{-1} \cdot \{\circ\} - k_1^2 \int_{\mathcal{V}_{\mathrm{O}}} \mathrm{d}^3 r' G_1(R)\, \overline{\boldsymbol{\alpha}}_e(\mathbf{r}') \cdot \{\circ\} - \nabla \int_{\mathcal{V}_{\mathrm{O}}} \mathrm{d}^3 r' G_1(R) \nabla' \cdot [\overline{\boldsymbol{\alpha}}_e(\mathbf{r}') \cdot \{\circ\}], \quad \mathbf{r} \in \mathcal{V}_{\mathrm{O}}, \quad (74)$$

$$q_{\mathrm{o}} \equiv \mathbf{D}_{\mathrm{o}}/(\varepsilon_1\sqrt{\eta_1}), \quad (75a)$$

$$F^{\mathrm{i}}_{\mathrm{o}} \equiv \mathbf{D}^{\mathrm{i}}_{\mathrm{o}}/(\varepsilon_1\sqrt{\eta_1}), \quad (75b)$$

Anisotropic magnetic body

$\mathsf{X}_{\mathrm{oo}} : \mathcal{V}_{\mathrm{O}} \to \mathcal{V}_{\mathrm{O}}$

(from flux density to flux density)

$$\mathsf{X}_{\mathrm{oo}}\{\circ\} \equiv \left[\frac{\overline{\boldsymbol{\mu}}_3(\mathbf{r})}{\mu_1}\right]^{-1} \cdot \{\circ\} - k_1^2 \int_{\mathcal{V}_{\mathrm{O}}} \mathrm{d}^3 r' G_1(R)\, \overline{\boldsymbol{\alpha}}_h(\mathbf{r}') \cdot \{\circ\} - \nabla \int_{\mathcal{V}_{\mathrm{O}}} \mathrm{d}^3 r' G_1(R) \nabla' \cdot [\,\overline{\boldsymbol{\alpha}}_h(\mathbf{r}') \cdot \{\circ\}], \quad \mathbf{r} \in \mathcal{V}_{\mathrm{O}}, \quad (76)$$

$$q_{\mathrm{o}} \equiv \mathbf{B}_{\mathrm{o}}\sqrt{\eta_1}/\mu_1, \quad (77a)$$

$$F^{\mathrm{i}}_{\mathrm{o}} \equiv \mathbf{B}^{\mathrm{i}}_{\mathrm{o}}\sqrt{\eta_1}/\mu_1, \quad (77b)$$

REFERENCES

[1] S. Bastonero, V. Lancellotti, and R. Orta, "Analysis of surface relief diffraction gratings made of anisotropic material," *Journal Optical and Quantum Electronics*, Oct. 1999.

[2] R. C. Rumpf, C. R. Garcia, H. H. Tsang, J. E. Padilla, and M. D. Irwin, "Electromagnetic isolation of a microstrip by embedding in a spatially variant anisotropic metamaterial," *Progress In Electromagnetics Research*, vol. 142, pp. 243–260, 2013.

[3] Z. H. Jiang, J. A. Bossard, X. Wang, and D. H. Werner, "Synthesizing metamaterials with angularly independent effective medium properties based on an anisotropic parameter retrieval technique coupled with a genetic algorithm," *Journal of Applied Physics*, vol. 109, no. 1, 2011.

[4] O. Sakai and K. Tachibana, "Plasmas as metamaterials: a review," *Plasma Sources Sci. Technol.*, vol. 21, p. 013001, 2012.

[5] D. Melazzi, V. Lancellotti, M. Manente, D. Pavarin, and T. Anderson, "Numerical investigation into the performance of a reconfigurable gaseous plasma antenna," in *8th European Conference on Antennas and Propagation (EuCAP 2014)*, (The Hague, The Netherlands), April 2014.

[6] D. Melazzi, V. Lancellotti, M. Manente, D. Pavarin, and T. Anderson, "An integral-equation approach to the analysis and design of plasma antennas," in *15th Int. Conf. on Electromagnetics in Advanced Applications (ICEAA '13)*, (Torino, Italy), pp. 716–719, Sept. 2013.

[7] D. Melazzi and V. Lancellotti, "ADAMANT: A surface and volume integral-equation solver for the analysis and design of Helicon plasma sources," *Computer Physics Communications*, vol. 185, pp. 1914–1925, 2014.

[8] P. Yla-Oijala, S. Kiminki, and S. Jarvenpaa, "Calderon preconditioned surface integral equations for composite objects with junctions," *IEEE Trans. Antennas Propag.*, vol. 59, pp. 546–554, Feb. 2011.

[9] Y. Ye, J. Yuan, and K. Su, "A volume-surface integral equation solver for radiation from microstrip antenna on anisotropic substrate," *International Journal of Antennas and Propagation*, 2012. 11 pages, Article ID 120208.

[10] J. Markkanen, C.-C. Lu, P. Ylä-Oijala, and A. Sihvola, "Mixed volume-surface integral equation solution for complex composite structures," in *2013 International Symposium on Electromagnetic Theory*, (Hiroshima, Japan), pp. 33–36, 2013.

[11] B. Usner, K. Sertel, M. Carr, and J. Volakis, "Generalized volume-surface integral equation for modeling inhomogeneities within high contrast composite structures," *IEEE Trans. Antennas Propag.*, vol. 54, pp. 68–75, Jan. 2006.

[12] E. J. Rothwell and M. J. Cloud, *Electromagnetics*. London: CRC Press, 2001.

[13] D. S. Jones, *The Theory of Electromagnetism*. Oxford: Pergamon, 1964.

[14] A. F. Peterson, S. L. Ray, and R. Mittra, *Computational Methods for Electromagnetics*. Piscataway: IEEE Press, 1998.

[15] A. J. Poggio and E. K. Miller, "Integral equation solutions of three dimensional scattering problems," in *Computer Techniques for Electromagnetics* (R. Mittra, ed.), pp. 159–264, Oxford, U.K.: Pergamon, 1973.

[16] P. Ylä-Oijala and M. Taskinen, "Well-conditioned Müller formulation for electromagnetic scattering by dielectric objects," *IEEE Trans. Antennas Propag.*, vol. 53, pp. 3316–3323, Oct. 2005.

[17] F. Andriulli, K. Cools, H. Bagci, F. Olyslager, A. Buffa, S. Christiansen, and E. Michielssen, "A multiplicative Calderon preconditioner for the electric field integral equation," *IEEE Trans. Antennas Propag.*, vol. 56, pp. 2398–2412, Aug. 2008.

[18] S. Kurz, O. Rain, and S. Rjasanow, "The adaptive cross-approximation technique for the 3D boundary-element method," *IEEE Trans. Magn.*, vol. 38, pp. 421–424, Mar. 2002.

[19] M. S. Tong, "Meshfree solutions of volume integral equations for electromagnetic scattering by anisotropic objects," *IEEE Trans. Antennas Propag.*, vol. 60, pp. 4249–4258, Sept. 2012.

[20] J. Markkanen, C.-C. Lu, X. Cao, and P. Yla-Oijala, "Analysis of volume integral equation formulations for scattering by high-contrast penetrable objects," *IEEE Trans. Antennas Propag.*, vol. 60, pp. 2367–2374, May 2012.

[21] S. Tao and R. Chen, "A higher-order solution of volume integral equation for electromagnetic scattering from inhomogeneous objects," *IEEE Antennas and Wireless Propagation Letters*, vol. 13, pp. 627–630, 2014.

[22] G. Kobidze and B. Shanker, "Integral equation based analysis of scattering from 3-D inhomogeneous anisotropic bodies," *IEEE Trans. Antennas Propag.*, vol. 52, no. 10, pp. 2650–2658, 2004.

[23] J. Markkanen, P. Yla-Oijala, and A. Sihvola, "Discretization of volume integral equation formulations for extremely anisotropic materials," *IEEE Trans. Antennas Propag.*, vol. 60, no. 11, pp. 5195–5202, 2012.

[24] K. Yang, J. C. Zhou, and M. S. Tong, "Inversion of electromagnetic scattering for 3D dielectric objects through integral equation method with Nyström discretization," *IEEE Trans. Antennas Propag.*, vol. 61, no. 6, pp. 3387–3392, 2013.

[25] B. Zhang, G. Xiao, J. Mao, and Y. Wang, "Analyzing large-scale non-periodic arrays with synthetic basis functions," *IEEE Trans. Antennas Propag.*, vol. 58, pp. 3576–3584, Nov. 2010.

[26] L. Matekovits, V. A. Laza, and G. Vecchi, "Analysis of large complex structures with the synthetic-functions approach," *IEEE Trans. Antennas Propag.*, vol. 55, pp. 2509–2521, Sep. 2007.

[27] H.-W. Yuan, S.-X. Gong, Y. Guan, and D.-Y. Su, "Scattering analysis of the large array antennas using the synthetic basis functions method," *J. Electromagn. Waves and Appl.*, vol. 23, no. 2-3, pp. 309–320, 2009.

[28] L. Matekovits, G. Vecchi, M. Bercigli, and M. Bandinelli, "Synthetic-functions analysis of large aperture-coupled antennas," *IEEE Trans. Antennas Propag.*, vol. 57, pp. 1936–1943, July 2009.

[29] W. Chen, G. Xiao, S. Xiang, and J. Mao, "A note on the construction of synthetic basis functions for antenna arrays," *IEEE Trans. Antennas Propag.*, vol. 60, pp. 3509–3512, July 2012.

[30] R. Maaskant, R. Mittra, and A. G. Tijhuis, "Fast analysis of large antenna arrays using the characteristic basis function method and the adaptive cross approximation algorithm," *IEEE Trans. Antennas Propag.*, vol. 56, pp. 3440–3451, Nov. 2008.

[31] L. Hu, L.-W. Li, and R. Mittra, "Electromagnetic scattering by finite periodic arrays using the characteristic basis function and adaptive integral methods," *IEEE Trans. Antennas Propag.*, vol. 58, pp. 3086–3090, Sept. 2010.

[32] J. Yuan, C. Gu, and G. Han, "A hybrid equivalent dipole moment and adaptive modified characteristic basis function method for electromagnetic scattering by multilayered dielectric bodies," *International Journal of RF and Microwave Computer-Aided Engineering*, vol. 19, pp. 685–691, Nov. 2009.

[33] J. Yeo, V. V. S. Prakash, and R. Mittra, "Efficient analysis of a class of microstrip antennas using the characteristic basis function method (CBFM)," *Microwave and Optical Technology Letters*, vol. 39, no. 6, pp. 456–464, 2003.

[34] C. Craeye, J. Laviada, R. Maaskant, and R. Mittra, "Macro basis function framework for solving Maxwells equations in surface-integral-equation form," *Forum for Electromagnetic Research Methods and Application Technologies (FERMAT)*, vol. 3, pp. 1–16, May 2014. Online at www.e-fermat.org.

[35] A. Yagbasan, C. Tunc, V. Erturk, A. Altintas, and R. Mittra, "Characteristic basis function method for solving electromagnetic scattering problems over rough terrain profiles," *IEEE Trans. Antennas Propag.*, vol. 58, pp. 1579–1589, May 2010.

[36] E. Lucente, A. Monorchio, and R. Mittra, "An iteration-free MoM approach based on excitation independent characteristic basis functions for solving large multiscale electromagnetic scattering problems," *IEEE Trans. Antennas Propag.*, vol. 56, pp. 999–1007, April 2008.

[37] J. Laviada, M. Pino, and F. Las-Heras, "Generation of excitation-independent characteristic basis functions for three-dimensional homogeneous dielectric bodies," *IEEE Trans. Antennas Propag.*, vol. 59, pp. 3318–3327, Sept 2011.

[38] L. Hu, L.-W. Li, and R. Mittra, "Electromagnetic scattering by finite periodic arrays using the characteristic basis function and adaptive integral methods," *IEEE Trans. Antennas Propag.*, vol. 58, pp. 3086–3090, Sept 2010.

[39] C. Delgado, E. Garcia, F. Catedra, and R. Mittra, "Generation of characteristic basis functions defined over large surfaces by using a multilevel approach," *IEEE Trans. Antennas Propag.*, vol. 57, pp. 1299–1301, April 2009.

[40] J. Laviada, F. Las-Heras, M. R. Pino, and R. Mittra, "Solution of electrically large problems with multilevel characteristic basis functions," *IEEE Trans. Antennas Propag.*, vol. 57, pp. 3189–3198, Oct. 2009.

[41] E. Garcia, C. Delgado, I. Diego, and M. Catedra, "An iterative solution for electrically large problems combining the characteristic basis function method and the multilevel fast multipole algorithm," *IEEE Trans. Antennas Propag.*, vol. 56, pp. 2363–2371, Aug 2008.

[42] M.-K. Li and W. C. Chew, "Multiscale simulation of complex structures using equivalence principle algorithm with high-order field point sampling scheme," *IEEE Trans. Antennas Propag.*, vol. 56, pp. 2389–2397, Aug. 2008.

[43] M.-K. Li and W. C. Chew, "Wave-field interaction with complex structures using equivalence principle algorithm," *IEEE Trans. Antennas Propag.*, vol. 55, pp. 130–138, Jan 2007.

[44] M.-K. Li and W. C. Chew, "Multiscale simulation of complex structures using equivalence principle algorithm with high-order field point sampling scheme," *IEEE Trans. Antennas Propag.*, vol. 56, pp. 2389–2397, Aug 2008.

[45] K. Zhang, J. OuYang, F. Yang, J. Zhang, and W. Luo, "Radiation pattern simulation of antenna array problem with perfectly electrically conducting object in arbitrary shape using novel hybrid method of equivalence principle algorithm and physical optics," *Microwaves, Antennas Propagation, IET*, vol. 8, pp. 217–227, March 2014.

[46] H. Shao, J. Hu, W. Lu, H. Guo, and Z. Nie, "Analyzing large-scale arrays using tangential equivalence principle algorithm with characteristic basis functions," *Proceedings of the IEEE*, vol. 101, pp. 414–422, Feb 2013.

[47] P. Ylä-Oijala and M. Taskinen, "Electromagnetic scattering by large and complex structures with surface equivalence principle algorithm," *Waves in Random and Complex Media*, vol. 19, pp. 105–125, Feb. 2009.

[48] G. Xiao, J.-F. Mao, and B. Yuan, "A generalized surface integral equation formulation for analysis of complex electromagnetic systems," *IEEE Trans. Antennas Propag.*, vol. 57, pp. 701–710, March 2009.

[49] D. J. Bekers, *Finite Antenna Arrays, an eigencurrent approach*. PhD thesis, Technische Universiteit Eindhoven, 2004.
[50] D. J. Bekers, S. J. L. van Eijndhoven, and A. G. Tijhuis, "An eigencurrent approach for the analysis of finite antenna arrays," *IEEE Trans. Antennas Propag.*, vol. 58, pp. 3772–3782, Dec. 2009.
[51] A. M. van de Water, B. P. de Hon, M. C. van Beurden, A. G. Tijhuis, and P. de Maagt, "Linear embedding via Green's operators: A modeling technique for finite electromagnetic band-gap structures," *Physics Review E*, vol. 72, pp. 1–11, Nov. 2005.
[52] D. J. Duque-Guerra, *Green's function diakoptics*. PhD thesis, Technische Universiteit Eindhoven, 2013.
[53] D. J. Duque-Guerra, V. Lancellotti, B. P. de Hon, and A. G. Tijhuis, "An efficient approach to the local optimization of finite electromagnetic band-gap structures," *Turk. J. Elec. Eng. & Comp. Sci.*, vol. 22, pp. 546–561, 2014.
[54] V. Lancellotti, B. P. de Hon, and A. G. Tijhuis, "An eigencurrent approach to the analysis of electrically large 3-D structures using linear embedding via Green's operators," *IEEE Trans. Antennas Propag.*, vol. 57, pp. 3575–3585, Nov. 2009.
[55] V. Lancellotti, B. P. de Hon, and A. G. Tijhuis, "Scattering from large 3-D piecewise homogeneous bodies through linear embedding via Green's operators and Arnoldi basis functions," *Progress In Electromagnetics Research*, vol. 103, pp. 305–322, April 2010.
[56] V. Lancellotti and A. G. Tijhuis, "Linear embedding via Green's operators," in *Computational Electromagnetics* (R. Mittra, ed.), pp. 227–257, Springer Science + Business Media: New York, 2014.
[57] V. Lancellotti and A. G. Tijhuis, "Mixed LEGO-EFIE approach for the analysis of radiating elements and anisotropic media," in *8th European Conference on Antennas and Propagation (EuCAP 2014)*, (The Hague, The Netherlands), pp. 2861–2865, April 2014. invited paper.
[58] V. Lancellotti and A. G. Tijhuis, "Solving wave propagation within finite-sized composite media with linear embedding via Green's operators," *Progress In Electromagnetics Research M*, vol. 25, pp. 127–140, July 2012.
[59] V. Lancellotti and A. G. Tijhuis, "Convergence properties of a diakoptics method for electromagnetic scattering from 3-D complex structures," *Progress In Electromagnetics Research M*, vol. 24, pp. 127–140, May 2012.
[60] V. Lancellotti, B. P. de Hon, and A. G. Tijhuis, "Wave scattering from random sets of closely spaced objects through linear embedding via Green's operators," *Waves in Random and Complex Media*, vol. 21, pp. 434–455, August 2011.
[61] V. Lancellotti, B. P. de Hon, and A. G. Tijhuis, "Analysis of antennas in the presence of large composite 3-D structures with linear embedding via Green's operators (LEGO) and a modified EFIE," in *4th European Conference on Antennas and Propagation (EuCAP '10)*, (Barcelona, SPAIN), pp. 1–5, April 2010. invited paper.
[62] V. Lancellotti and A. G. Tijhuis, "Extended linear embedding via Green's operators for analyzing wave scattering from anisotropic bodies," *International Journal of Antennas and Propagation*, 2014. 11 pages, Article ID 467931.
[63] X. Yuan, "Three-dimensional electromagnetic scattering from inhomogeneous objects by the hybrid moment and finite element method," *IEEE Transactions on Microwave Theory and Techniques*, vol. 38, pp. 1053–1058, Aug. 1990.
[64] M.-L. Yang, H.-W. Gao, W. Song, and X.-Q. Sheng, "An effective domain-decomposition-based preconditioner for the FE-BI-MLFMA method for 3D scattering problems," *IEEE Trans. Antennas Propag.*, vol. 62, pp. 2263–2268, April 2014.
[65] D. Bau III and L. N. Trefethen, *Numerical linear algebra.* Philadelphia: Soci. Indus. Ap. Math., 1997.
[66] V. Lancellotti, B. P. de Hon, and A. G. Tijhuis, "On the convergence of the eigencurrent expansion method applied to linear embedding via Green's operators (LEGO)," *IEEE Trans. Antennas Propag.*, vol. 58, pp. 3231–3238, Oct. 2010.
[67] R. W. P. King, *The Theory of Linear Antennas*. Cambridge, MA: Harvard University Press, 1956.
[68] C. A. Balanis, *Antenna Theory: Analysis and Design*. New York: John Wiley & Sons, Inc., second ed., 1997.
[69] A. E. H. Love, "The integration of the equations of propagation of electric waves," *Philos. Trans. R. Soc. London, Ser. A*, vol. 197, pp. 1–45, 1901.
[70] D. Pozar, *Microwave Engineering*. New York: Wiley, 1998.
[71] R. E. Collin, *Foundations for Microwave Engineering*. New York: McGraw-Hill, 1992.
[72] S. M. Rao, D. R. Wilton, and A. W. Glisson, "Electromagnetic scattering by surfaces of arbitrary shape," *IEEE Trans. Antennas Propag.*, vol. 30, pp. 409–418, May 1982.
[73] D. H. Schaubert, D. R. Wilton, and A. W. Glisson, "A tetrahedral modeling method for electromagnetic scattering by arbitrarily shaped inhomogeneous dielectric bodies," *IEEE Trans. Antennas Propag.*, vol. 32, no. 1, pp. 77–85, 1984.
[74] T. Anderson, *Plasma Antennas*. Artech House, 2011.
[75] I. Alexeff, T. Anderson, S. Parameswaran, E. Pradeep, J. Hulloli, and P. Hulloli, "Experimental and theoretical results with plasma antennas," *IEEE Trans. Antennas Propag.*, vol. 32, no. 2, pp. 166–172, 2006.
[76] T. Stix, *Plasma Waves*. Springer-Verlag, NewYork Inc., 1992.

Vito Lancellotti received the laurea (M. Sc.) degree with honors in Electrical Engineering and the Ph.D. degree in Electronics and Communications both from Politecnico di Torino, Italy, in 1995 and 1999, respectively. In early 1999 he joined Telecom Italia Lab in Torino as a Senior Researcher and was involved in projects concerning TCP/IP and ATM networks. In June 2000 again as a Senior Researcher he joined the Milan-based subsidiary of Corning (now Avanex), where he worked on broadband electro-optic lithium niobate modulators and optical waveguides. From 2002 to 2008 he served as a Research Fellow and Professor under grant in the Department of Electrical Engineering of Politecnico di Torino, where he substantively contributed to the development of the TOPICA code, devised for analysis and design of plasma facing antennas for magnetically controlled nuclear fusion. In 2005 he was appointed Visiting Scientist at Massachusetts Institute of Technology, Cambridge (MA), and in 2007 spent a research period at Max-Planck-Institut fur Plasmaphysik, Garching (Germany). As of April 2008 he has been with Department of Electrical Engineering of Eindhoven University of Technology, The Netherlands, where he currently serves as an Assistant Professor. His current research interests concern efficient techniques for the computational modeling of electromagnetic fields in large and complex structures, plasma-based antennas and devices, and interaction of EM waves with biological tissues.

Davide Melazzi received a M.Sc. degree in Aerospace Engineering and a Ph.D. degree in Space Science and Technology from University of Padova, Italy, in 2008 and 2013, respectively. In 2009, he developed with Dr. Johan Carlsson (Tech-X Corp., USA) a full-wave electromagnetic code for magnetized plasma columns for the design of Helicon plasma thrusters (under the FP7 grant 218862, HPH.com project). In 2010 and 2011, he was a visiting Ph.D. at the Technical University of Eindhoven (Eindhoven, the Netherlands), where with Dr. Lancellotti he developed the ADAMANT code for the electromagnetic simulation of RF antennas facing plasmas. In 2012, he was a visiting Ph.D. at ENEA-EURATOM (Frascati, Italy), where with Dr. Cardinali he analyzed wave propagation and absorption mechanism in magnetized plasma sources. Since 2013, he has been with the Department of Industrial Engineering, University of Padova (Padova, Italy) as a PostDoc Fellow. His current research interests concern plasma antennas, plasma metamaterials, and magnetized plasma sources.